

# Comparing the ACS/WFC and WFC3/UVIS Calibration and Photometry

---

S.E. Deustua and J. Mack  
March 12, 2018

---

## ABSTRACT

*A study was undertaken using synthetic photometry of CALSPEC stars to compare the ACS Wide Field Channel (WFC) photometry to the WFC3 UVIS imaging channel in eight similarly named passbands corresponding to the broadband filters F435W (ACS/WFC) F438W (WFC3/UVIS) and F475W, F555W, F606W, F625W, F775W, F814W and F850LP (both ACS/WFC and WFC3/UVIS). The uncertainty of the photometric calibration of ACS/WFC and WFC3/UVIS with respect to the white dwarf standard stars is within  $\pm 0.5\%$  for F814W, F775W, F606W and F475W, and within  $\pm 1\%$  for F625W and F850LP. For F555W the apparent difference in the calibration is 2% for F555W and 6% for UVIS/F438W and ACS/F435W due to inherent differences in the filter passbands. Comparing the ACS/WFC to WFC3/UVIS mean flux for stars having a range of spectral types shows a color dependence. The WFC to UVIS F814W color dependence is  $\pm 0.02$  mags for F814W, F775W, F475W and F606W. For the other filters the range is -0.06 to +0.02 mags. Aperture photometry of the 47 Tucanae cluster confirm the results from using synthetic photometry of CALSPEC stars.*

---

## 1. Introduction

The Advanced Camera for Surveys (ACS) was installed in the Hubble Space Telescope (HST) in 2002. Its instrument complement consists of the Wide Field Channel (WFC), the High Resolution Channel (HRC) and the Solar Blind Channel (SBC). Wide Field Camera 3 (WFC3) was installed in HST in 2009, replacing the WFPC2 (Wide Field Planetary Camera) and consists of a UV to Visible (UVIS) channel and an infrared (IR) channel. Detailed descriptions of the instruments are available from the ACS and WFC3 Instrument and Data Handbooks, as well as their respective

webpages and Instrument Science Reports. To date, ACS/WFC (?) has over 54,000 imaging datasets and WFC3/UVIS over 35,000 imaging datasets.

Many science programs take advantage of the two instruments' complementarity, and some programs exploit the capability afforded by acquiring parallel, simultaneous observations with both instruments. Between the two instruments, the most similar channels are the ACS/WFC and the WFC3/UVIS. Both have two 2048x4096 pixel CCDs. The former has a field of view of 202 x 202 arcseconds, resolution of 0.05 arcsec/pixel, and, a spectral response between 0.35 and 1.1 micrometers; the latter has a 162 x 162 arcsecond field of view, 0.04 arcsec/pixel resolution, and, spectral response between 0.2 and 1.0 micrometers. ACS/WFC and WFC3/UVIS also have similar bandpass names for eight broad band filters, namely, F435W, F475W, F555W, F606W, F625W, F775W, F814W, F850LP for ACS/WFC and F438W, F475W, F555W, F606W, F625W, F775W, F814W, F850LP for WFC3/UVIS. The similarities lead naturally to the question of how well do the photometric calibration for the two instruments compare. Details of each instrument's calibration are contained in numerous ISRs which are listed in the reference section of this report.

## 2. ACS/WFC and WFC3/UVIS System Bandpasses.

System bandpasses for each of the eight filters, F435W, F475W, F555W, F606W, F625W, F775W, F814W, F850LP for ACS/WFC and F438W, F475W, F555W, F606W, F625W, F775W, F814W, F850LP for WFC3/UVIS, were computed using PySynphot. System bandpasses include

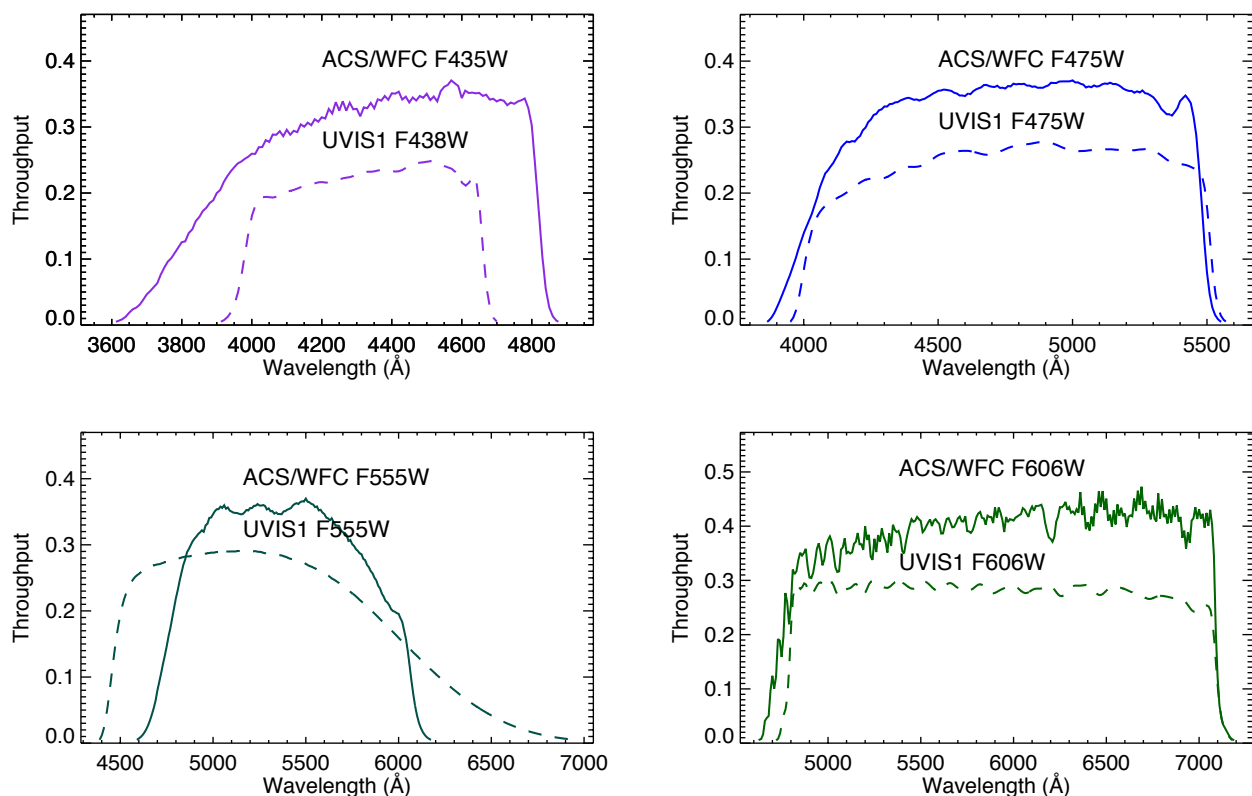


Figure 1 System bandpasses for the ACS/WFC filters (solid lines) and the WFC3/UVIS1 filters (dashed lines). Throughputs are derived using PySynphot. While the names of the filters are the same, the bandpasses of the two instruments have different transmission functions.

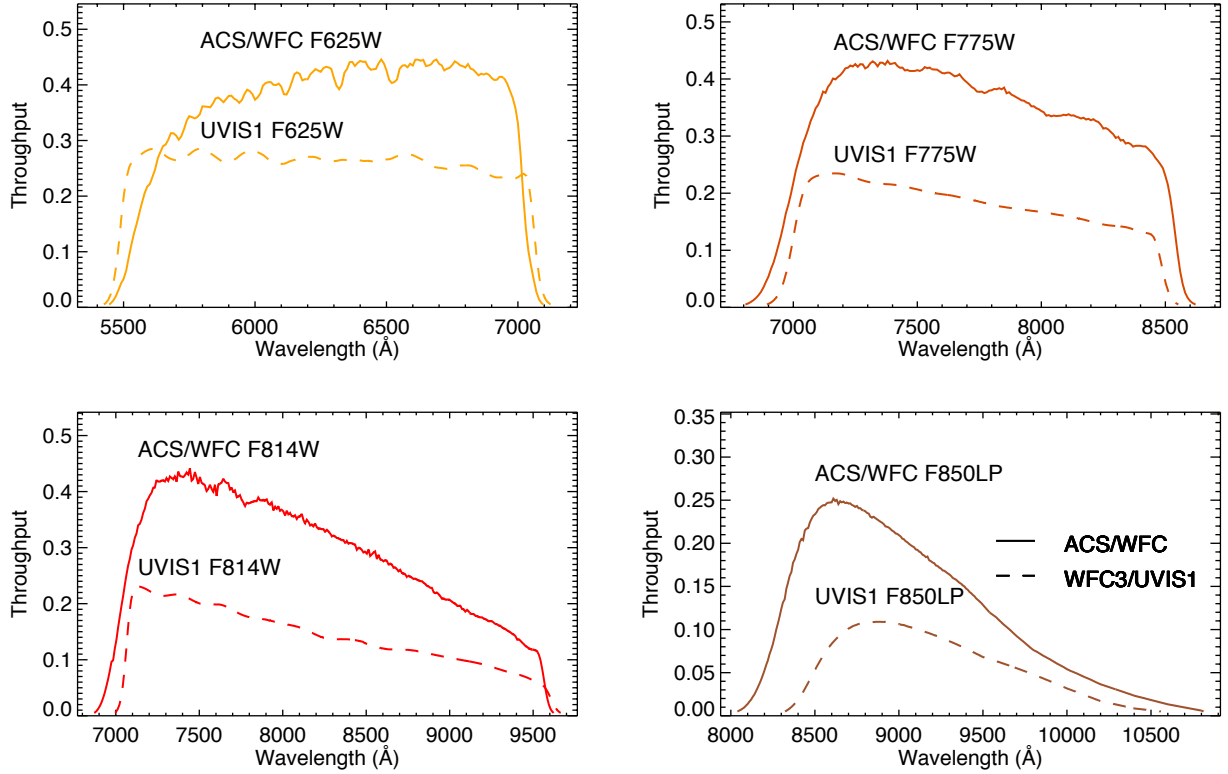


Figure 2. System bandpasses for the ACS/WFC filters (solid lines) and the WFC3/UVIS1 filters (dashed lines). Throughputs are derived using PySynphot. While the names of the filters are the same, the bandpasses of the two instruments have different transmission functions.

the filter transmission as well as the spectral response of the OTA (Optical Telescope Assembly), instrument optics and detector quantum efficiency. The throughput curves for each bandpass are shown in Figure 1 where the ACS/WFC bandpasses are shown as solid lines and the WFC3/UVIS1 bandpasses are shown as dashed lines. Although the ACS/WFC channel also has two CCDs, the synthetic photometry tables for WFC1 and WFC2 are identical, i.e. the response curves are the same; hence the generic use of ACS/WFC for that instrument.

### 3. Method and Analysis

With the objective of comparing the photometric systems of ACS/WFC to WFC3/UVIS camera with as direct an approach as possible, spectra of well characterized stars were chosen for this study. Thus, 26 spectra for stars with a range of spectral types and brightness were selected from from the CALSPEC database (<http://www.stsci.edu/hst/observatory/crds/calspec.html>). Spectral energy distributions (SED) chosen are hot white dwarfs, including the three primary white dwarf standard stars, GD153, GD71 and G191B2B, A stars, including Vega and Sirius, G stars and several cool late-type stars. The primary white dwarf standards are used to calibrate the system response for the ACS and WFC3 cameras (cf. Deustua et al. 2017, Bohlin 2014). Vega and Sirius are the fundamental standards and have SI-traceable pedigrees; Vega to Hayes and Latham (1975) and Sirius to Price et al. (2004). A review of absolute astronomical standards is in Deustua, Smith and Tucker. Spectral type, brightness, name of the CALSPEC spectrum file and the CALSPEC name of the star sample are listed in Table 1.

| Star Name               | CALSPEC<br>Name | Sp.<br>Type | V Mag  | CALSPEC Spectrum File |
|-------------------------|-----------------|-------------|--------|-----------------------|
| BD+02d3375              | bd02d3375       | A5          | 9.93   | bd02d3375_stis_003    |
| BD+33d2642              | bd21d0607       | B2IV        | 10.83  | bd21d0607_stis_003    |
| BD+26d2606              | bd26d2606       | A5          | 9.73   | bd26d2606_stis_003    |
| BD+29d2091              | bd29d2091       | F5          | 10.22  | bd29d2091_stis_003    |
| BD+54d1216              | bd54d1216       | sdF6        | 9.71   | bd54d1216_stis_003    |
| HD009051                | hd009051        | G7III       | 8.92   | hd009051_stis_003     |
| HD031128                | hd031128        | F4V         | 9.14   | hd031128_stis_003     |
| HD074000                | hd074000        | sdF6        | 9.66   | hd074000_stis_003     |
| HD111980                | hd111980        | F7V         | 8.38   | hd111980_stis_003     |
| HD160617                | hd160617        | F           | 8.73   | hd160617_stis_003     |
| HD185975                | hd185975        | G3V         | 8.1    | hd185975_stis_003     |
| HD200654                | hd200654        | G           | 9.11   | hd200654_stis_003     |
| 2MASSJ17571324+6703409  | 1757132         | A3V         | 12.01  | 1757132_stis_004      |
| 2MASSJ18083474+6927286  | 1808347         | A3V         | 11.69  | 1808347_stis_004      |
| BD+60d1753              | bd60d1753       | A1V         | 9.65   | bd60d1753_stis_004    |
| HD106252                | hd106252        | G0          | 7.36   | hd106252_stis_004     |
| HD116405                | hd116405        | A0V         | 8.34   | hd116405_stis_004     |
| HD14943                 | hd14943         | A5V         | 5.91   | hd14943_stis_004      |
| HD158485                | hd158485        | A4V         | 6.5    | hd158485_stis_004     |
| HD159222                | hd159222        | G1V         | 6.56   | hd159222_stis_004     |
| HD163466                | hd163466        | A6V         | 6.85   | hd163466_stis_004     |
| HD180609                | hd180609        | A0V         | 9.42   | hd180609_stis_004     |
| HD205905                | hd205905        | G2V         | 6.74   | hd205905_stis_004     |
| HD37725                 | hd37725         | A3          | 8.31   | hd37725_stis_004      |
| HD37962                 | hd37962         | G2V         | 7.85   | hd37962_stis_004      |
| HD38949                 | hd38949         | G1V         | 7.8    | hd38949_stis_004      |
| Ksi2 Ceti               | ksi2ceti        | B9III       | 4.28   | ksi2ceti_stis_004     |
| Lam Lep                 | lamlep          | B0.5IV      | 4.27   | lamlep_stis_004       |
| 2MASSJ17403468+6527148  | 1740346         | A6V         | 12.48  | 1740346_stisnic_004   |
| BD+21d0607              | bd17d4708       | F2          | 9.22   | bd17d4708_stisnic_006 |
| AGK+81266               | agk_81266       | sdO         | 11.95  | agk_81266_stisnic_006 |
| 10 Lac                  | 10lac           | O9V         | 4.88   | 10lac_stis_004        |
| 2MASS J17325264+7104431 | 1732526         | A4V         | 12.21  | 1732526_stisnic_004   |
| 2MASS J17430448+6655015 | 1743045         | A8III       | 13.525 | 1743045_stisnic_004   |
| 2MASS J18022716+6043356 | 1802271         | A2V         | 11.985 | 1802271_stisnic_004   |
| 2MASS J18052927+6427520 | 1805292         | A4V         | 12.74  | 1805292_stisnic_004   |
| 2MASS J18120957+6329423 | 1812095         | A5V         | 12.01  | 1812095_stisnic_004   |
| ALPHA LYR (VEGA)        | alpha_lyr       | A0V         | 0.03   | alpha_lyr_stis_008    |
| Feige 110               | feige110        | sdO         | 11.83  | feige110_stisnic_006  |

| Star Name               | CALSPEC<br>Name | Sp.<br>Type | V Mag    | CALSPEC Spectrum File   |
|-------------------------|-----------------|-------------|----------|-------------------------|
| G191B2B                 | g191b2b         | DA          | 11.69    | g191b2b_stisnic_006     |
| GD153                   | gd153           | DA          | 13.349   | gd153_stisnic_006       |
| GD71                    | gd71            | DA          | 13.032   | gd71_stisnic_006        |
| GRW +70 5824            | grw_70d5824     | DA          | 12.773   | grw_70d5824_stisnic_007 |
| HD165459                | hd165459        | A4V         | 6.86     | hd165459_stisnic_004    |
| Mu Col                  | mucol           | O9.5V       | 5.15     | mucol_stis_004          |
| 2MASS J15591357+4736419 | p177d           | G0V         | 12.917   | p177d_stisnic_007       |
| 2MASS J16313382+3008465 | p330e           | G0V         | 13.52    | p330e_stisnic_008       |
| 2MASSJ14515797+7143173  | p041c           | GOV         | 12.16    | po41c_stisnic_007       |
| ALPHA CMA (SIRIUS)      | sirius          | A1V         | -1.46    | sirius_stis_002         |
| 2MASS J16293576+5255532 | snap1           | SdBO        | 15.4     | snap1_stisnic_006       |
| 2MASS J16194609+5534178 | snap2           | G           | 15.4     | snap2_stisnic_007       |
| Sun                     | sun_reference   | G2V         | -26.75   | sun_reference_stis_002  |
| WD 1057 +719            | wd1057_719      | DA          | 14.68    | wd1057_719_stisnic_006  |
| WD 1657 +343            | wd1657_343      | DA          | g=16.139 | wd1657_343_stisnic_006  |

Table 1. List of stars used in the analysis. The first column is a common SIMBAD name, the second column the CALSPEC name. Other columns are spectral type, brightness (in V mag except where noted otherwise), and the name of the CALSPEC spectrum file.

### A. Comparing the Photometric Calibrations of ACS/WFC and WFC3/UVIS

Because the calibration of the two instruments is based on the same three stars, the system throughputs and synthetic photometry tables are expected to be similar to within the measurement and instrument uncertainties (i.e. knowledge of instrument behavior). Therefore, it is reasonable to check the photometric calibration (i.e. the system response of each instrument) using the standard stars. First, the mean flux at the effective wavelength was computed for each star for the infinite aperture using its CALSPEC spectrum and the synthetic photometry tables for each instrument. For WFC3, these tables correspond to the May 2016 version for the chip-dependent calibration (Deustua et al. 2016 and Deustua et al. 2017) and for ACS/WFC these are the Bohlin (2016) tables. Calculations were carried out individually for UVIS1 and for UVIS2 and compared separately to the results for ACS/WFC.

The results of the PySynphot synthetic photometry calculation are listed in Table 2 for the three primary white dwarfs, and also for Vega (Alpha Lyrae) and Sirius (Alpha Canis Majoris), where the first column is the star name, the second column lists the WFC3 and ACS filters respectively, columns 3, 5, and 7 list the effective wavelength for the target in the passband, and columns 4, 6 and 8 list the mean flux in the passband. Figure 3 shows the CALSPEC spectral energy distributions for each of the primary white dwarf standards; the synthetic mean flux at the effective wavelength is plotted as red crosses for ACS/WFC and blue open diamonds for WFC3/UVIS1. The results for UVIS2 are identical to those for UVIS1.

| Star    | Bandpass       | WFC3/UVIS1                  |   | WFC3/UVIS2                  |   | ACS/WFC                     |   | WFC /<br>UVIS1<br>Flux ratio | WFC /<br>UVIS2<br>Flux Ratio |
|---------|----------------|-----------------------------|---|-----------------------------|---|-----------------------------|---|------------------------------|------------------------------|
|         |                | $\lambda_{\text{eff}}$<br>Å | $F_{\lambda}$<br>erg s <sup>-1</sup> cm <sup>-2</sup> Å <sup>-1</sup> | $\lambda_{\text{eff}}$<br>Å | $F_{\lambda}$<br>erg s <sup>-1</sup> cm <sup>-2</sup> Å <sup>-1</sup> | $\lambda_{\text{eff}}$<br>Å | $F_{\lambda}$<br>erg s <sup>-1</sup> cm <sup>-2</sup> Å <sup>-1</sup> |                              |                              |
| G191B2B | F438W or F435W | 4308.28                     | 1.69743E-13   | 4307.09                     | 1.69904E-13   | 4287.25                     | 1.70301E-13   | 1.003                        | 1.002                        |
|         | F475W          | 4690.06                     | 1.20034E-13   | 4688.65                     | 1.20153E-13   | 4665.02                     | 1.22404E-13   | 1.020                        | 1.019                        |
|         | F555W          | 5190.05                     | 8.13400E-14   | 5189.35                     | 8.13873E-14   | 5307.27                     | 7.67928E-14   | 0.944                        | 0.944                        |
|         | F606W          | 5716.51                     | 5.51278E-14   | 5714.74                     | 5.51943E-14   | 5742.96                     | 5.40281E-14   | 0.980                        | 0.979                        |
|         | F625W          | 6163.13                     | 4.30334E-14   | 6162.42                     | 4.30528E-14   | 6245.54                     | 4.10657E-14   | 0.954                        | 0.954                        |
|         | F775W          | 7599.33                     | 1.94748E-14   | 7596.76                     | 1.95022E-14   | 7634.88                     | 1.91077E-14   | 0.981                        | 0.980                        |
|         | F814W          | 7919.70                     | 1.62417E-14   | 7911.63                     | 1.63089E-14   | 7919.41                     | 1.62789E-14   | 1.002                        | 0.998                        |
|         | F850lp         | 9132.34                     | 9.58470E-15   | 9128.02                     | 9.60439E-15   | 8960.32                     | 1.02804E-14   | 1.073                        | 1.070                        |
| GD153   | F438W or F435W | 4311.86                     | 3.84548E-14   | 4310.67                     | 3.84871E-14   | 4294.39                     | 3.84376E-14   | 1.000                        | 0.999                        |
|         | F475W          | 4697.23                     | 2.75966E-14   | 4695.84                     | 2.76219E-14   | 4672.59                     | 2.81039E-14   | 1.018                        | 1.017                        |
|         | F555W          | 5194.30                     | 1.90128E-14   | 5193.59                     | 1.90236E-14   | 5311.05                     | 1.79787E-14   | 0.946                        | 0.945                        |
|         | F606W          | 5722.04                     | 1.29426E-14   | 5720.27                     | 1.29578E-14   | 5748.27                     | 1.26932E-14   | 0.981                        | 0.980                        |
|         | F625W          | 6163.20                     | 1.01714E-14   | 6162.49                     | 1.01759E-14   | 6245.48                     | 9.70670E-15   | 0.954                        | 0.954                        |
|         | F775W          | 7599.94                     | 4.65010E-15   | 7597.37                     | 4.65662E-15   | 7635.49                     | 4.56272E-15   | 0.981                        | 0.980                        |
|         | F814W          | 7920.84                     | 3.88074E-15   | 7912.75                     | 3.89672E-15   | 7920.45                     | 3.88952E-15   | 1.002                        | 0.998                        |
|         | F850lp         | 9133.62                     | 2.29652E-15   | 9129.31                     | 2.30125E-15   | 8961.64                     | 2.46142E-15   | 1.072                        | 1.070                        |
| GD71    | F438W or F435W | 4314.64                     | 5.03060E-14   | 4313.45                     | 5.03440E-14   | 4300.16                     | 5.00866E-14   | 0.996                        | 0.995                        |
|         | F475W          | 4701.89                     | 3.64489E-14   | 4700.53                     | 3.64804E-14   | 4677.62                     | 3.70809E-14   | 1.017                        | 1.016                        |
|         | F555W          | 5196.95                     | 2.53907E-14   | 5196.24                     | 2.54049E-14   | 5313.68                     | 2.40217E-14   | 0.946                        | 0.946                        |
|         | F606W          | 5725.98                     | 1.73270E-14   | 5724.21                     | 1.73471E-14   | 5752.00                     | 1.70025E-14   | 0.981                        | 0.980                        |
|         | F625W          | 6163.17                     | 1.36834E-14   | 6162.46                     | 1.36894E-14   | 6245.37                     | 1.30580E-14   | 0.954                        | 0.954                        |
|         | F775W          | 7600.37                     | 6.30384E-15   | 7597.79                     | 6.31264E-15   | 7636.01                     | 6.18611E-15   | 0.981                        | 0.980                        |
|         | F814W          | 7921.88                     | 5.26618E-15   | 7913.79                     | 5.28772E-15   | 7921.54                     | 5.27817E-15   | 1.002                        | 0.998                        |
|         | F850lp         | 9133.95                     | 3.12886E-15   | 9129.62                     | 3.13522E-15   | 8962.22                     | 3.35240E-15   | 1.071                        | 1.069                        |

| Star   | Bandpass       | WFC3/UVIS1                  |   | WFC3/UVIS2                  |   | ACS/WFC                     |   | WFC /<br>UVIS1<br>Flux Ratio | WFC /<br>UVIS2<br>Flux Ratio |
|--------|----------------|-----------------------------|---|-----------------------------|---|-----------------------------|---|------------------------------|------------------------------|
|        |                | $\lambda_{\text{eff}}$<br>Å | $F_{\lambda}$<br>erg s <sup>-1</sup> cm <sup>-2</sup> Å <sup>-1</sup> | $\lambda_{\text{eff}}$<br>Å | $F_{\lambda}$<br>erg s <sup>-1</sup> cm <sup>-2</sup> Å <sup>-1</sup> | $\lambda_{\text{eff}}$<br>Å | $F_{\lambda}$<br>erg s <sup>-1</sup> cm <sup>-2</sup> Å <sup>-1</sup> |                              |                              |
| Sirius | F438W or F435W | 4323.56                     | 2.62413E-08   | 4322.4                      | 2.62538E-08   | 4341.91                     | 2.50453E-08   | 0.954                        | 0.954                        |
|        | F475W          | 4730.31                     | 2.03858E-08   | 4729.02                     | 2.03985E-08   | 4707.56                     | 2.06207E-08   | 1.012                        | 1.011                        |
|        | F555W          | 5231.69                     | 1.53249E-08   | 5230.93                     | 1.53319E-08   | 5330.88                     | 1.47331E-08   | 0.961                        | 0.961                        |
|        | F606W          | 5776.65                     | 1.11846E-08   | 5774.84                     | 1.11951E-08   | 5805.05                     | 1.10141E-08   | 0.985                        | 0.984                        |
|        | F625W          | 6185.1                      | 9.32516E-09   | 6184.37                     | 9.32847E-09   | 6263.91                     | 8.98122E-09   | 0.963                        | 0.963                        |
|        | F775W          | 7614.35                     | 4.91953E-09   | 7611.68                     | 4.92538E-09   | 7650.97                     | 4.84177E-09   | 0.984                        | 0.983                        |
|        | F814W          | 7971.72                     | 4.27250E-09   | 7963.18                     | 4.28607E-09   | 7967.84                     | 4.27650E-09   | 1.001                        | 0.998                        |
|        | F850lp         | 9166.83                     | 2.94258E-09   | 9162.31                     | 2.94716E-09   | 9003.22                     | 3.06535E-09   | 1.042                        | 1.040                        |
| Vega   | F438W or F435W | 4323.73                     | 6.66684E-09   | 4322.56                     | 6.66997E-09   | 4342.21                     | 6.35756E-09   | 0.954                        | 0.953                        |
|        | F475W          | 4732.62                     | 5.20190E-09   | 4731.33                     | 5.20507E-09   | 4709.79                     | 5.26025E-09   | 1.011                        | 1.011                        |
|        | F555W          | 5235.55                     | 3.93243E-09   | 5234.78                     | 3.93421E-09   | 5332.49                     | 3.78694E-09   | 0.963                        | 0.963                        |
|        | F606W          | 5782.3                      | 2.89320E-09   | 5780.48                     | 2.89586E-09   | 5811.18                     | 2.84962E-09   | 0.985                        | 0.984                        |
|        | F625W          | 6188.26                     | 2.42386E-09   | 6187.53                     | 2.42470E-09   | 6266.64                     | 2.33743E-09   | 0.964                        | 0.964                        |
|        | F775W          | 7615.99                     | 1.29988E-09   | 7613.31                     | 1.30139E-09   | 7652.4                      | 1.27931E-09   | 0.984                        | 0.983                        |
|        | F814W          | 7977.1                      | 1.13318E-09   | 7968.49                     | 1.13666E-09   | 7972.75                     | 1.13398E-09   | 1.001                        | 0.998                        |
|        | F850lp         | 9171.24                     | 7.92198E-10   | 9166.71                     | 7.93326E-10   | 9008.71                     | 8.21994E-10   | 1.038                        | 1.036                        |

Table 2 Mean flux density and effective wavelength computed for the primary standard stars through the eight similar passbands for WFC3/UVIS1, WFC3/UVIS2 and ACS/WFC. The mean flux ( $F_{\lambda}$ ) ratio of WFC to UVIS1 and WFC to UVIS2 are listed in the last two columns, respectively. The synthetic photometry is for the CALSPEC spectral energy distributions of the stars listed in Table 1

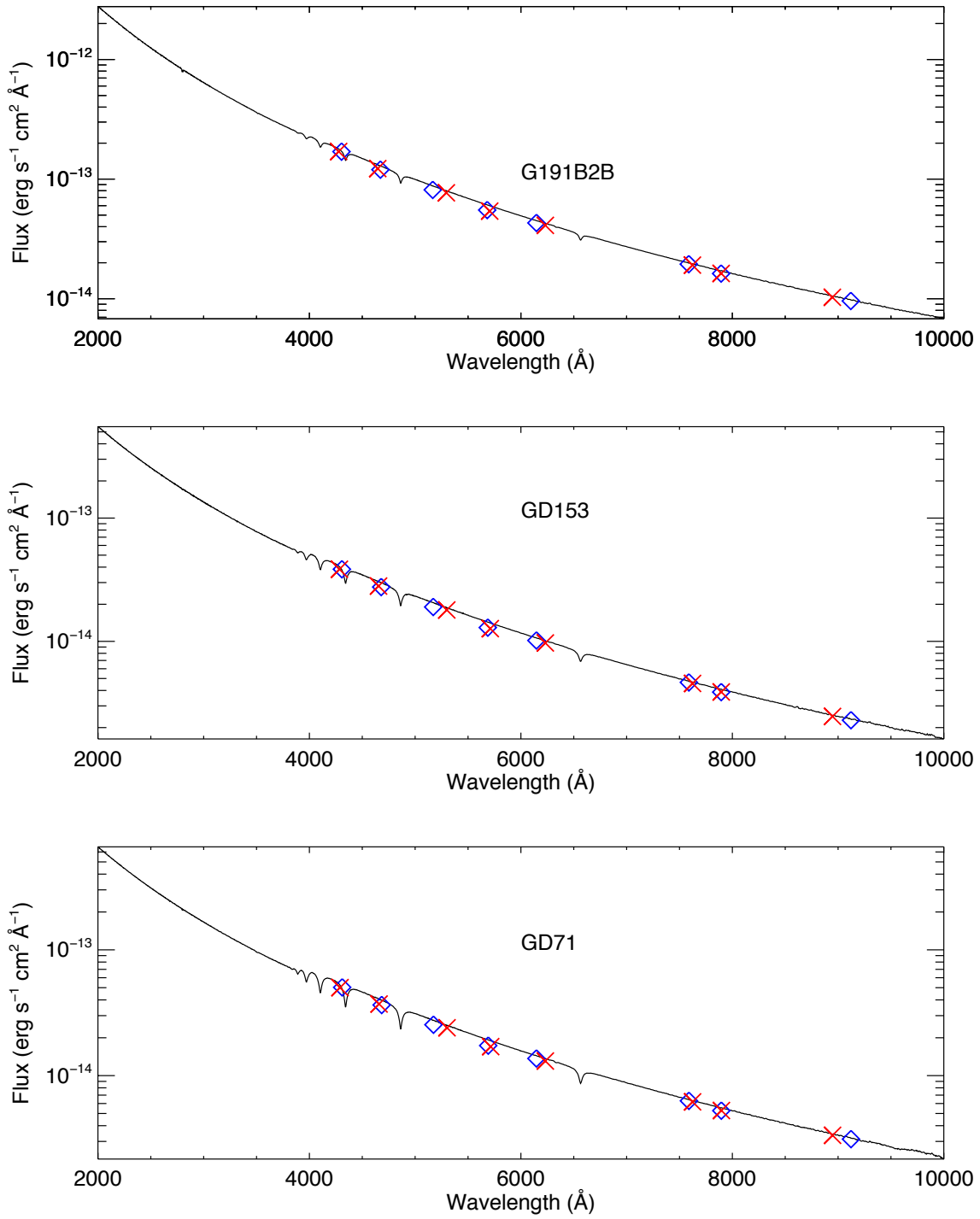


Figure 3. Spectral energy distributions of the three primary HST white dwarf standards, G191B2B, GD153 and GD71 used to derive the photometric calibration for both instruments. The mean flux at the effective wavelength for each bandpass, computed using the synthetic photometry tables and the CALSPEC spectrum is indicated by red crosses for ACS/WFC and by open blue diamonds for WFC3/UVIS1.



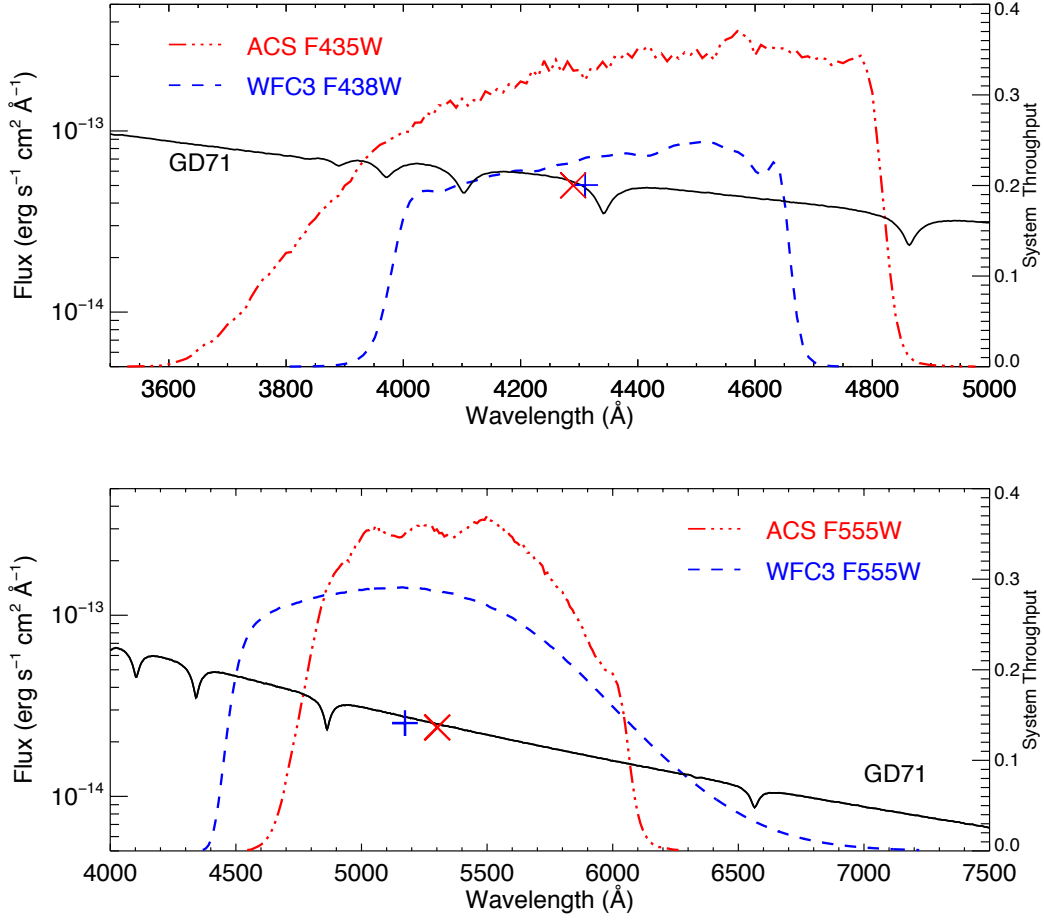


Figure 4. The effect of bandpass throughputs is illustrated in these two plots where the ACS bandpass (red dash dotted line), the WFC3 bandpass (blue dashed line), GD71’s spectrum (solid black line) and the mean flux at the effective wavelengths (blue plus for WFC3, red cross for ACS) are shown. The upper plot shows the wavelength region for F435W (ACS) and F438W (WFC3), and the lower, for F555W for ACS and WFC3. A consequence of the effect of the system throughput is that the effective wavelengths are not coincident: e.g. for F555W, the ACS effective wavelength is longer than for WFC3, but the opposite is the case for the bluer filters (F435W and F438W).

The difference in the synthetic photometry mean flux is always lower than the spectral flux at the effective wavelength due to the presence of spectral absorption features. The difference in effective wavelength in the two instruments (ACS/WFC and WFC3/UVIS) for the similarly named filters is due to the different bandpass shapes. A closeup of two wavelength regions, one centered around 4300 Å and the other at about 5500 Å, is shown in Figure 4. This shows the effect of bandpass transmission and spectral energy distribution: Effective wavelengths in each matched pair of ACS and WFC3/UVIS1 bandpasses are notably different from each other in the F555W filters, but more similar in the F435W/F438W pair (which have more similar bandpass shapes). Figure 5 uses a cartoon to better illustrate this effect, where we use a model square bandpass and an spectral energy distribution with and without spectral features.

For each of the ACS and WFC3 filters, the ratio of the stellar monochromatic flux at the effective wavelength to the synthetic mean monochromatic flux i.e.  $F_{\lambda}(\text{CALSPEC})/F_{\lambda}(\text{SYN})$ , is computed

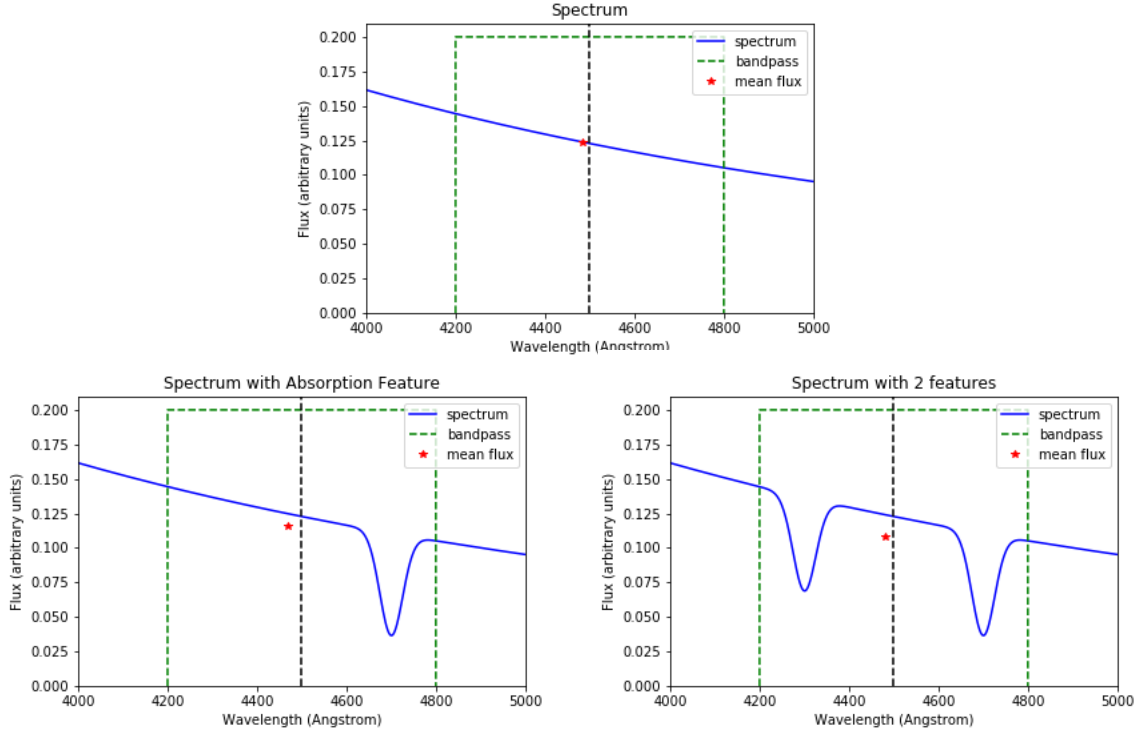


Figure 5. The top panel shows a model box bandpass (green dashed line) and a model spectrum (solid blue line). The vertical dashed black line is the bandpass central wavelength. The red star is the position of the mean flux of the spectrum at the effective wavelength. On the lower left is a spectrum with one absorption feature, and, on the lower right, one with two absorption lines. In both examples, the mean flux is lower and the effective wavelength is offset from the black line.

for the each of the white dwarfs, and then the ratios are averaged. In Figure 6, the CALSPEC to synthetic ratio is plotted versus effective wavelength, where the ratio varies from  $\sim 0.94$  to 1.07.

To check the ACS and WFC3 photometric calibration we looked at the fractional difference between the CALSPEC/SYN ratios for bandpass pairs, as shown in Figure 7. Where the bandpasses are most similar, i.e. shape, width and effective wavelengths are similar, the agreement between the two instruments mean flux is excellent, to 0.5% or better. Where the bandpasses have significantly different transmission functions the fractional difference is large:  $\sim 2.5\%$  for F555W and 5.5% for F435W/F438W (see Figure 1). For the latter, the effective wavelengths are in or near the wings of the 4341Å Balmer absorption line (see Figure 4) and hence their mean flux is less similar.

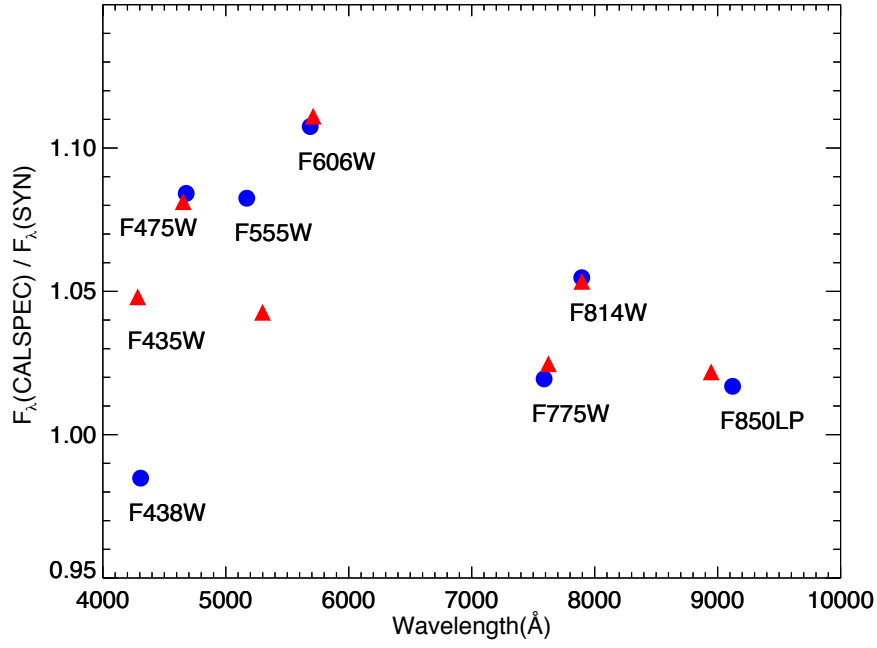


Figure 6. The average ratio of the CALSPEC stellar monochromatic flux density at the bandpass effective wavelength to the synthetic mean flux density within the bandpass for the white dwarf standards (G191B2B, GD71 and GD153). ACS/WFC values are designated by the red triangles, and the WFC3/UVIS1 values are denoted by the blue circles.

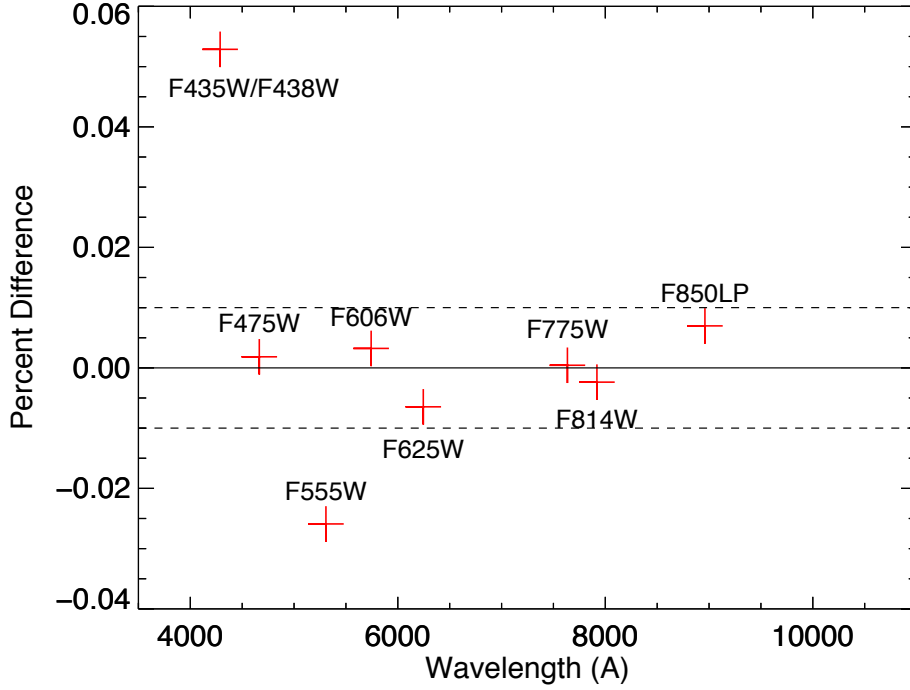


Figure 7. The difference (ACS minus UVIS) in the average mean CALSPEC/PySynphot flux ratios shown in Figure 6 for the 8 passbands of this study plotted against the bandpass effective wavelengths. The dashed lines mark +1% and -1%. Agreement of the mean flux where the passbands are most similar in the two instruments is excellent, better than  $\pm 0.5\%$ . The apparent difference between F435W/F438W and F555W is a consequence of dissimilar transmission functions.

## B. Color difference between ACS/WFC and WFC3/UVIS within bandpasses

Second, we use CALSPEC stars to directly compare the instrument-to-instrument colors in the ‘same’ filter (i.e. in bandpass pairs). The selection of CALSPEC stars was made with the main criterion of full wavelength coverage in both ACS/WFC and WFC3/UVIS. Applying this criterion provided 57 stars. We compute the mean flux for CALSPEC stars in each passband and instrument channel (i.e. ACS/WFC, WFC3/UVIS1 and WFC3/UVIS2), convert to Vega magnitudes by dividing by the mean Vega flux in each passband i.e.  $\text{VegaMag}(\text{star}) = -2.5 \log(F(\text{star})/F(\text{Vega}))$ . Then the WFC-UVIS magnitude difference was calculated for each pair of passbands, e.g. WFC F435W – UVIS F438W, WFC F475W – UVIS F475W etc. ACS/WFC stellar colors for F435W-F814W, F435W-F606W and F606W-F814W are also calculated. All these results are tabulated, per star, in Table 4 for WFC -UVIS1 and in Table 7 for WFC -UVIS2, both of which are found in the Appendix. Plots of stellar color vs. instrument color for WFC-UVIS1 are shown in Figure 8 and for WFC-UVIS2 in Figure 13 (in the Appendix).

From Figure 8 it is apparent that instrument color and stellar color are correlated, with one notable exception. For F814W there is virtually no correlation with stellar spectral type and almost no magnitude difference ( $\Delta\text{mag} \sim -0.001$ ) between the ACS/WFC and WFC3/UVIS filters.

For six of the bandpasses, F475W, F555W, F606W, F625W, F775W and F814W the relationship between instrument color and stellar color is linear. For F850LP, there is not a simple linear fit, and we use three separate line segments, depending on stellar color. Where the ACS/WFC and WFC3/UVIS bandpasses are most similar in terms of overall shape and blue and red edges e.g. F814W, F775W, F606W and F475W, the color dependence on the magnitude difference is smaller. Conversely, where the bandpasses are significantly different in either shape or filter edges, the color effect is more pronounced.

The extreme example is the difference between WFC F435W and UVIS1 F438W where a high order polynomial fit worked best. The UVIS F438W bandpass is significantly narrower compared to that of WFC F435W; its blue edge is at a longer wavelength (i.e. redder) and the red edge is at a shorter wavelength (bluer), and the slope of the blue side of the bandpasses are noticeably different (see Figure 1). Regardless of spectral type, all stars appear bluer in the WFC bandpass compared to UVIS1, though red stars less so, as is indicated by the shallower slope for  $(F435W-F814W) > 0$  in the upper left panel of Figure 8a. The F850LP bandpasses have a similar relationship as F435W and F438W. We divided the F850LP vs. ACS color data into three regions, and fit each with a line.

The WFC3/UVIS1 F850LP bandpass has blue and red edges that lie within the ACS/WFC bandpass. However, the peaked effect seen in the F435W/F438W plot is absent since at these wavelengths the Rayleigh-Jeans tails of hot stars ( $T > 5000$ ) are nearly parallel, whereas the spectral energy distributions of cool stars are still rising (see Figure 9).

The coefficients (intercept and slope) and their corresponding uncertainties for the linear fits are listed in the Appendix in Table 5 for WFC-UVIS1 and in Table 8 for WFC-UVIS2. Table 6 gives the coefficients for the F850LP bandpass (WFC-UVIS1), and Table 9 the same for WFC-UVIS2.

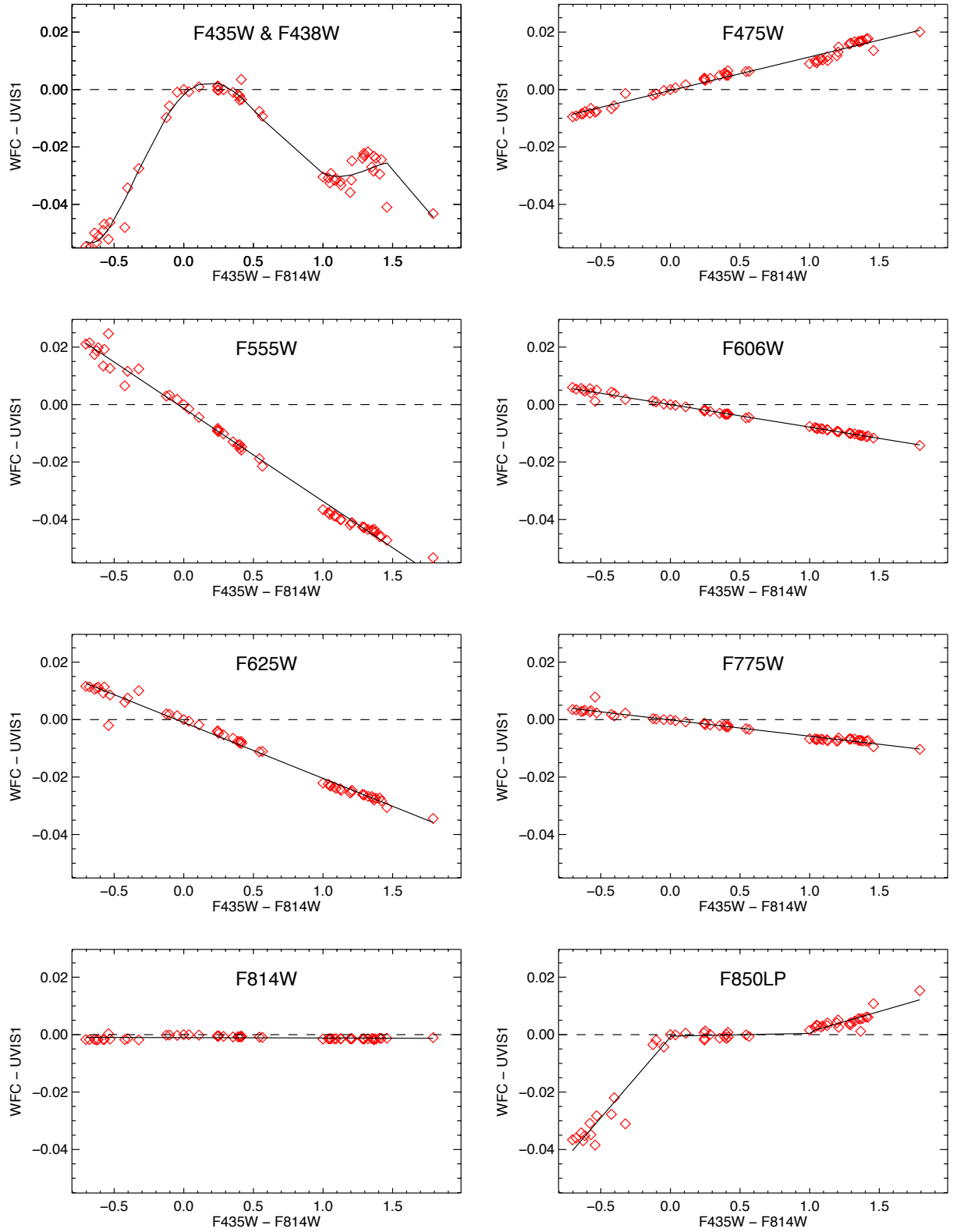


Figure 8a. Plots of stellar color (ACS F435W-F814W) versus the difference between the ACS/WFC and WFC3/UVIS1 magnitudes for each of the similar bandpasses in the Vegamag system. The relationship is linear except for F435W-F438W where a 5<sup>th</sup> order polynomial was used, and, F850LP where a 3-line fit

seemed appropriate.

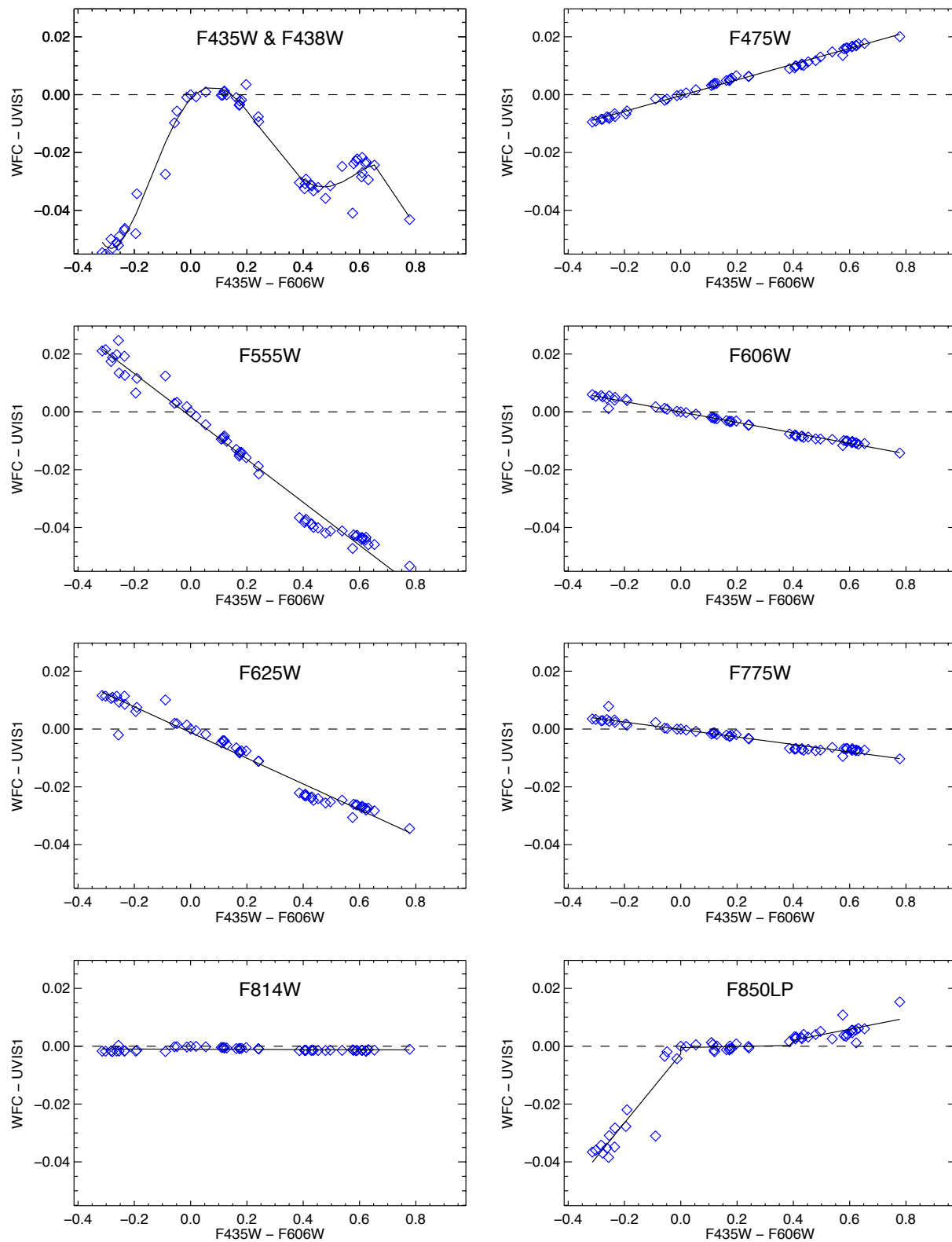


Figure 8b. As in Figure 8a but plotted against ACS/WFC F435W -F606W, roughly comparable to B-V

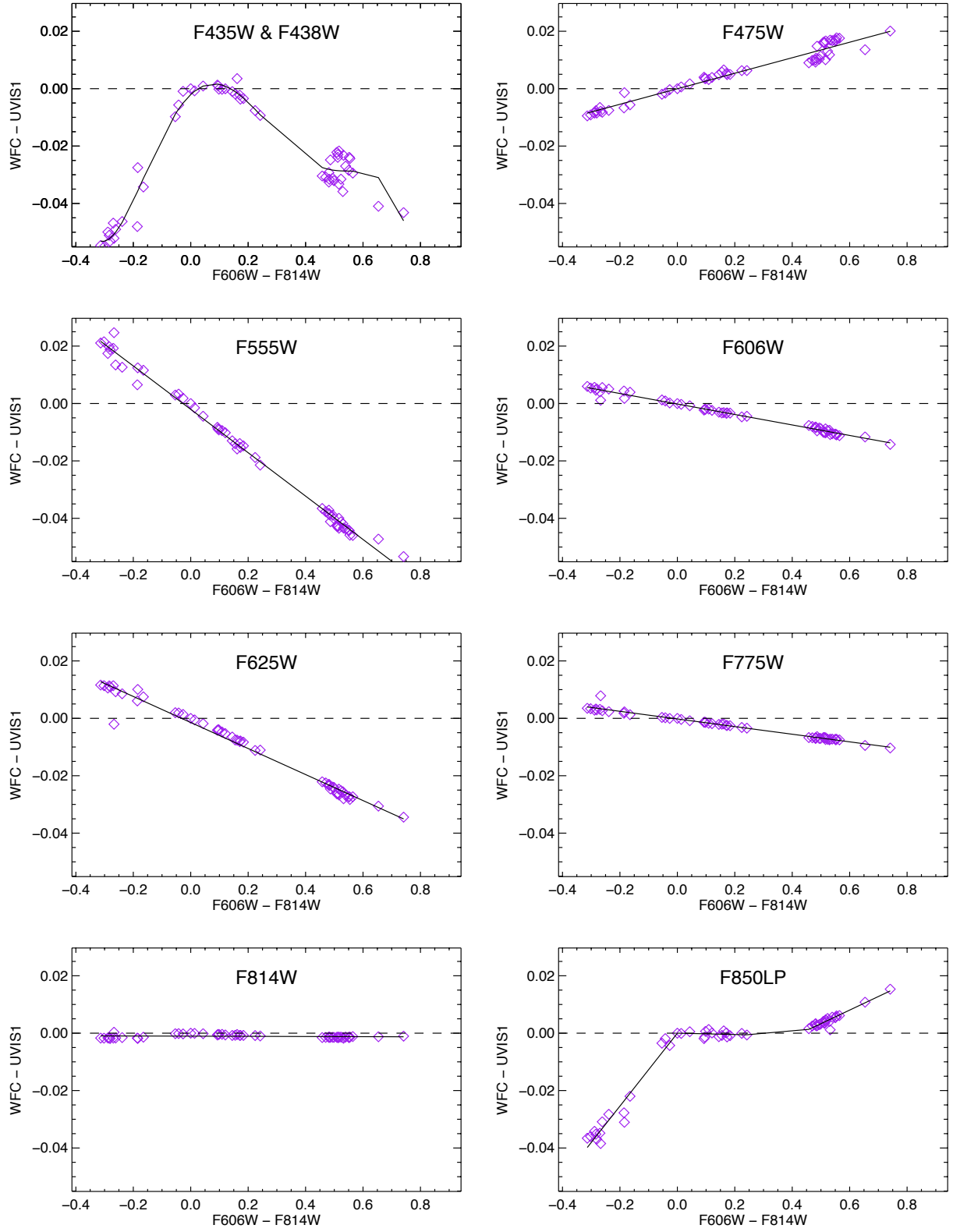


Figure 8c. As in Figure 8a but plotted against ACS/WFC F606W-F814W, roughly like V-I.

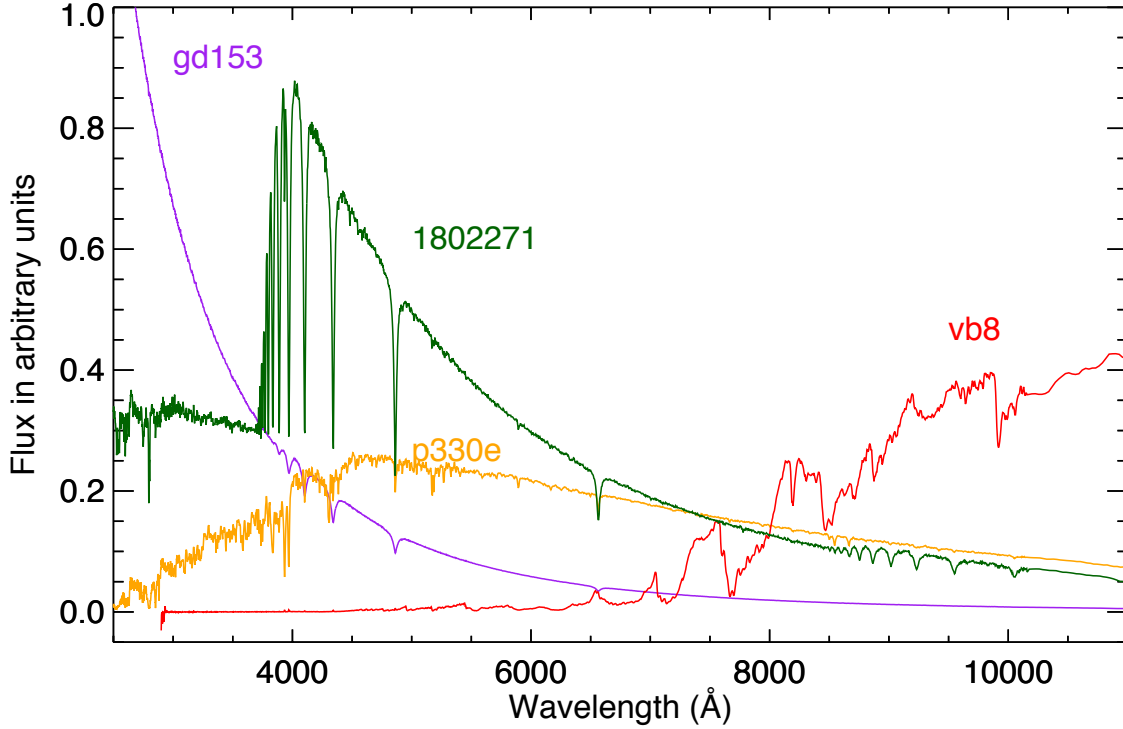


Figure 9 CALSPEC spectra of four representative stars: a hot, white dwarf GD153, the A dwarf star 18022716, a cooler G dwarf star P330E and the cool M dwarf VB8, showing a range of spectral energy distributions in the wavelength range of the ACS Wide Field Camera ‘s broad band filters.

Thus far, the discussion of cross instrument photometry has been limited to the case of individual stars and synthetic photometric values. In the next section, we use observations of the globular cluster 47 Tucanae, obtained in with the ACS/WFC and WFC3/UVIS imagers, as a case study of cross instrument photometry.

### C. Case Study of Cross-Instrument Photometry: 47 Tucanae

Aperture photometry of the globular cluster 47 Tucanae was used to compute relative photometry between the WFC3/UVIS and ACS/WFC detectors. Until 2016, the WFC3/UVIS photometric calibration followed the ACS/WFC philosophy of providing a single calibration for the focal plane, but in 2016, the WFC3/UVIS team implemented a chip dependent solution, wherein each CCD was calibrated independently. The WFC3 team found that the original, ‘one chip’ photometric calibration differed by 3-4% from the ‘new’ chip dependent solution. Our original goal was to show that the latest UVIS photometric calibration (Deustua et al., 2017) brings the computed WFC3/UVIS magnitudes in agreement to the current ACS/WFC photometric system.

For this comparison, ACS observations were selected from calibration program 10737, which was designed to monitor the stability of the ACS Wide Field Camera CCD sensitivity with time. These consist of 3 repeated exposures (339 seconds each) at the same position on the sky in both F606W and in F814W, as described in Table 3. The individual exposures in each filter were combined



| Detector<br>Program | Filter | Date     | #exp | Exptime<br>(sec) | Rootname   | Dither<br>X, Y | Zpt@0.5"<br>(current) | Zpt@0.5"<br>(2012)  |
|---------------------|--------|----------|------|------------------|------------|----------------|-----------------------|---------------------|
| ACS 10737           | F606W  | Nov2005  | 3    | 339              | j9irw1*flc | 0, 0"          | 26.585 <sup>a</sup>   | --                  |
|                     | F814W  | Nov2005  | 3    | 339              | j9irw1*flc | 0, 0"          | 26.694 <sup>b</sup>   | --                  |
| WFC3 11452          | F606W  | Jul 2009 | 9    | 350              | iaby01*flc | ±40, ±40"      | 26.173 <sup>c</sup>   | 26.143 <sup>e</sup> |
|                     | F814W  | Jul 2009 | 9    | 350              | iaby01*flc | ±40, ±40"      | 25.844 <sup>d</sup>   | 25.882 <sup>f</sup> |

<sup>a</sup> ACS F606W STMAG@0.5" = STMAG@infin + apcor(0.5"/infin) = 26.681+2.5\*log(0.915/1.000) = 26.585

<sup>b</sup> ACS F814W STMAG@0.5" = STMAG@infin + apcor(0.5"/infin) = 26.792+2.5\*log(0.914/1.000) = 26.694

<sup>c</sup> UVIS F606W STMAG@0.5" = STMAG@0.4"- apcor(0.4"/0.5") = 26.154-2.5\*log(0.910/0.926) = 26.173

<sup>d</sup> UVIS F814W STMAG@0.5" = STMAG@0.4"- apcor(0.4"/0.5") = 25.823-2.5\*log(0.903/0.921) = 25.844

<sup>e</sup> UVIS F606W STMAG@0.5" = STMAG@0.4"- apcor(0.4"/0.5") = 26.124-2.5\*log(0.910/0.926) = 26.143

<sup>f</sup> UVIS F814W STMAG@0.5" = STMAG@0.4"- apcor(0.4"/0.5") = 25.861-2.5\*log(0.903/0.921) = 25.882

Table 3: ACS/WFC and WFC3/UVIS observations of 47 Tucanae used to derive relative photometry between the two detectors. Footnotes in the ‘Zpt’ columns show how the STMAG zeropoint at 0.5" is computed for both detectors using both the latest photometric calibration and the prior 2012 UVIS solution which was in place before the chip-dependent calibration.

with AstroDrizzle in order to reject artifacts and to improve the overall signal-to-noise. For the UVIS detector, observations of 47 Tucanae were selected from the WFC3 calibration program 11452, where 9 dithered exposures were obtained in each filter to validate the accuracy of the spatial sensitivity (flat fields) on-orbit. These data overlap the same region of sky as the ACS calibration field and reach a similar depth, having exposures times of 350 seconds each. Because the dithered offsets for each exposure were large (~25% of the UVIS field of view), TweakReg was used to improve the alignment via the image header world coordinate system before drizzling each UVIS filter to match the combined ACS mosaics.

In order to make the most straightforward comparison between the two detectors, photometry was performed using the large 0.5 arcsec standard ACS aperture, the radius at which the PSF becomes insensitive to temporal and spatial variations across the detector. This reduces the chance of making any systematic errors in deriving encircled energy corrections for each exposure in this crowded cluster field, which are required when using smaller apertures. The sky background was computed as the mode in a small annulus between 0.52-0.64 arcsec. To minimize the photometric scatter due to crowding effects, only isolated sources (eg. no neighbors within a radius of 0.6 arcsec) were selected. Additionally, only stars with photometric errors less than ~1% (0.01 mag) were used for the analysis.

While the standard aperture for WFC3 is a bit smaller than ACS at 0.4 arcsec, UVIS photometry was performed with the same 0.5 arcsec aperture in order to sample the same area on the sky for each detector. For ACS, the STMag zeropoints defined for an infinite aperture (Bohlin 2016) were corrected for the encircled energy fraction from 0.5" to infinity, as described in the footnotes of Table 3. For WFC3, the 0.4 arcsec STMag zeropoints were used, with a correction for the encircled energy from 0.4 to 0.5 arcsec (Deustua et al., 2017). The STMag system was selected over the VegaMag system for this test, with the goal of eliminating any systematic uncertainties in the calibration of Vega.

Relative photometry (ACS/WFC minus WFC3/UVIS) is plotted in Figure 10 for F814W and in Figure 11 for F606W, where the top panel corresponds to the UVIS1 chip and the bottom panel to the UVIS2 chip. Points in black correspond to photometry using the 2012 UVIS calibration (Kalirai et al 2012, which are available only on the WFC3 website [http://www.stsci.edu/hst/wfc3/analysis/uvis\\_zpts/2012\\_UVIS\\_ZeroPoints\\_infinite.jpg](http://www.stsci.edu/hst/wfc3/analysis/uvis_zpts/2012_UVIS_ZeroPoints_infinite.jpg)) which was in place prior to the chip-dependent 2017 calibration shown in red. For the F814W filter, the difference (ACS – UVIS1) is nearly flat over a range of  $\sim 2.5$  magnitudes, and the average offset has been reduced from  $0.030 \pm 0.015$  mag in 2012 to  $-0.006 \pm 0.015$  mag in 2017. The F814W bandpass is nearly identical in shape for the ACS and WFC3 detectors, with virtually no difference in the predicted magnitude with spectral type, as demonstrated by the synthetic photometry from Figure 8. This difference is overplotted as a function of stellar magnitude in bins of 0.5 mag and varies by only  $\sim 0.002$  mag over the full brightness range. The F814W chip 2 difference (ACS-UVIS2) shows a similar flat distribution with magnitude, with an average offset of  $0.035 \pm 0.015$  mag in 2012 and  $-0.002 \pm 0.015$  mag in 2017, suggesting a slight residual offset in photometry  $\sim 0.004$  mag between the two UVIS chips.

For the F606W filter, Figure 11 shows that relative photometry (ACS-UVIS) is not flat over the range of stellar magnitude sampled. For the brightest bin (STMAG=19), which is just below saturation, the mean offset is very close to zero at  $-0.005 \pm 0.020$  mag for UVIS1 and  $0.000 \pm 0.022$  mag for UVIS2. This difference increases as the stars decrease in brightness, with the faintest bin (STMAG=21.0) offset by  $-0.016 \pm 0.022$  mag for UVIS1 and  $-0.014 \pm 0.02$  mag for UVIS2. To determine the color range sampled by this range of brightness, the F606W and F814W photometric catalogs were matched by position and used to create a color-magnitude diagram (F606W-F814W) vs F814W in the ACS STMag system.

This CMD is plotted in Figure 12 using the same the F814W magnitude range shown in Figure 10 (eg. the depth required to limit the photometric errors to  $<0.01$  magnitude). This corresponds to a total range in color (V-I) of approximately 0.6 magnitudes for stars along the main sequence. A second population of sources appears to the right of the main sequence, and these are most likely binary stars which are  $\sim$ twice as bright, or 0.75 mag above the main sequence. For the majority of isolated stars in 47 Tucanae, however, sampling sources of varying brightness is equivalent to sampling sources of varying color, with brighter stars on the main sequence being representatively bluer.

The F606W relative photometry in Figure 11 is therefore consistent with the predictions from synthetic photometry in Figure 8, which shows that bandpass differences between the ACS/WFC and WFC3/UVIS detectors mean that the two systems agree for blue sources but diverge linearly with color by up to a few hundredths of a magnitude for redder sources. Since the calibration of the UVIS detector was based primarily on observations of white dwarf standards, the agreement in the two systems for blue sources is within expectations.

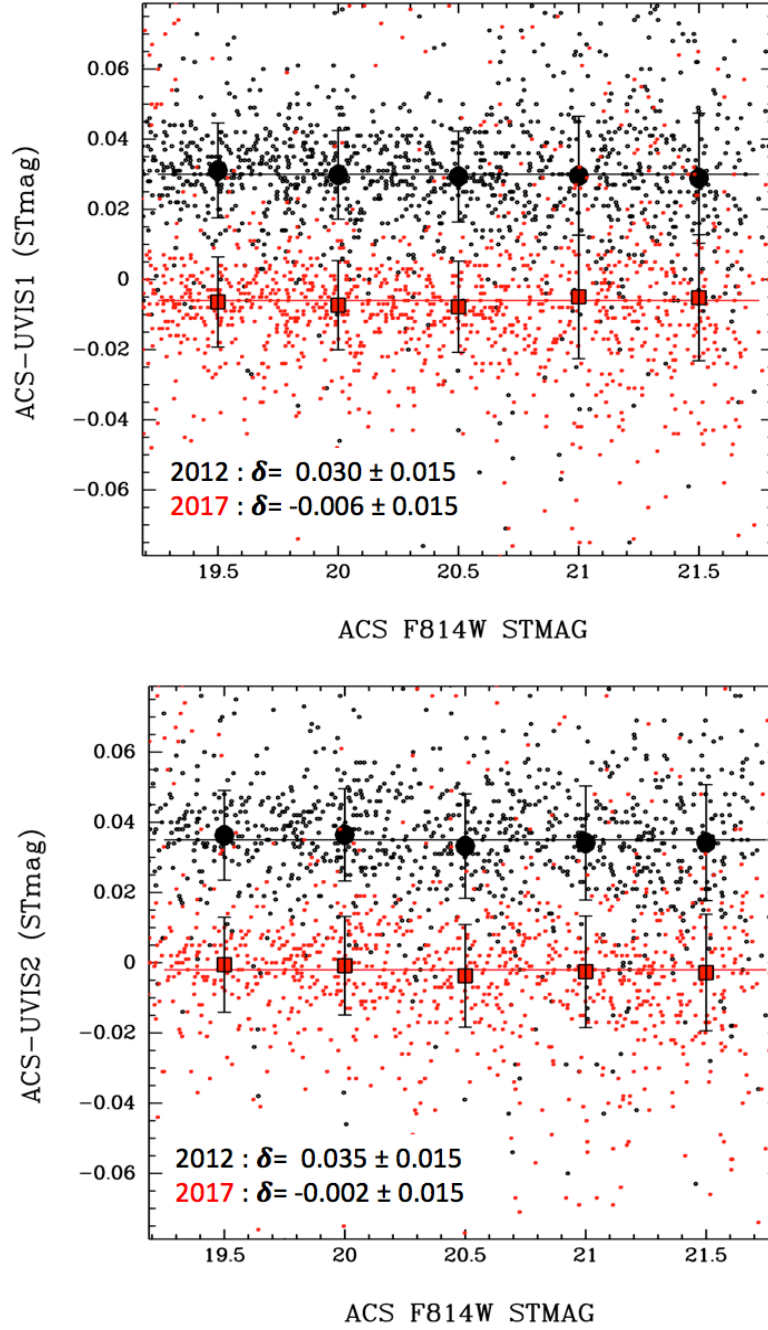


Figure 10. F814W STMAG difference (ACS-UVIS) using the 2012 UVIS photometric calibration (black) and the 2017 calibration (red). The two UVIS chips are plotted in the upper and lower panels, respectively. The mean offset is over-plotted as a straight line for each solution and is closer to zero with the new calibration over a range of  $\sim 2.5$  magnitudes.

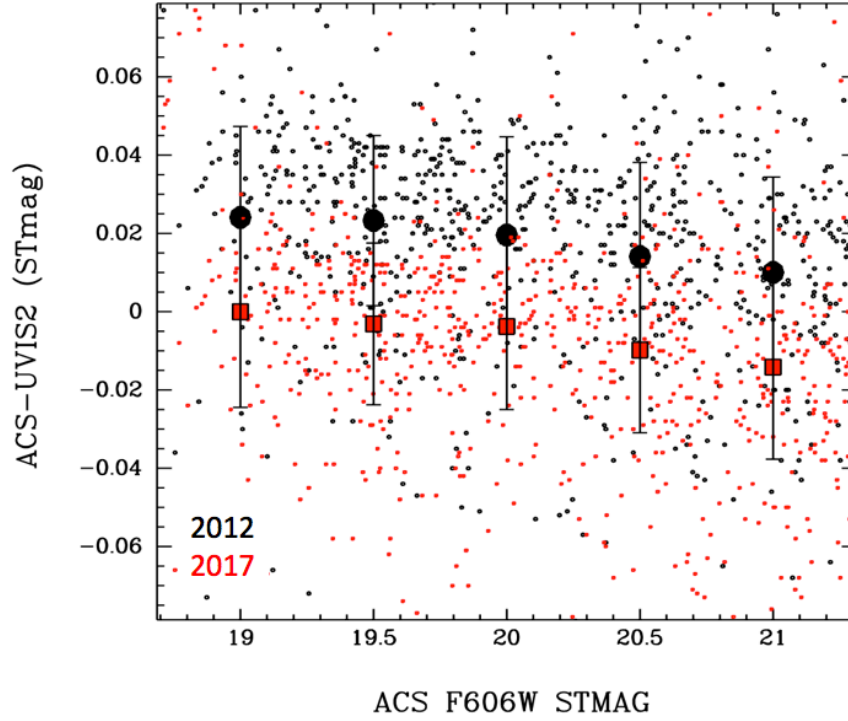
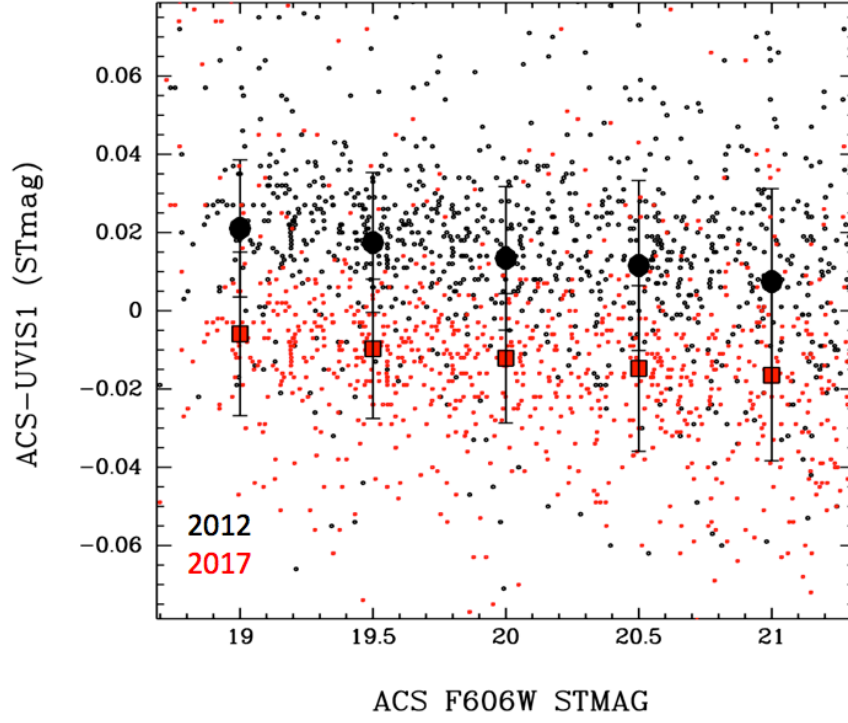


Figure 11. F606W STMAG difference (ACS-UVIS) using the 2012 UVIS photometric calibration (black) and the 2017 calibration (red). The two UVIS chips are plotted in the upper and lower panels, respectively. The mean 2017 offset is very close to zero for the brightest (bluer) sources, and this difference increases to  $\sim 0.015$  magnitudes for fainter (redder) sources.

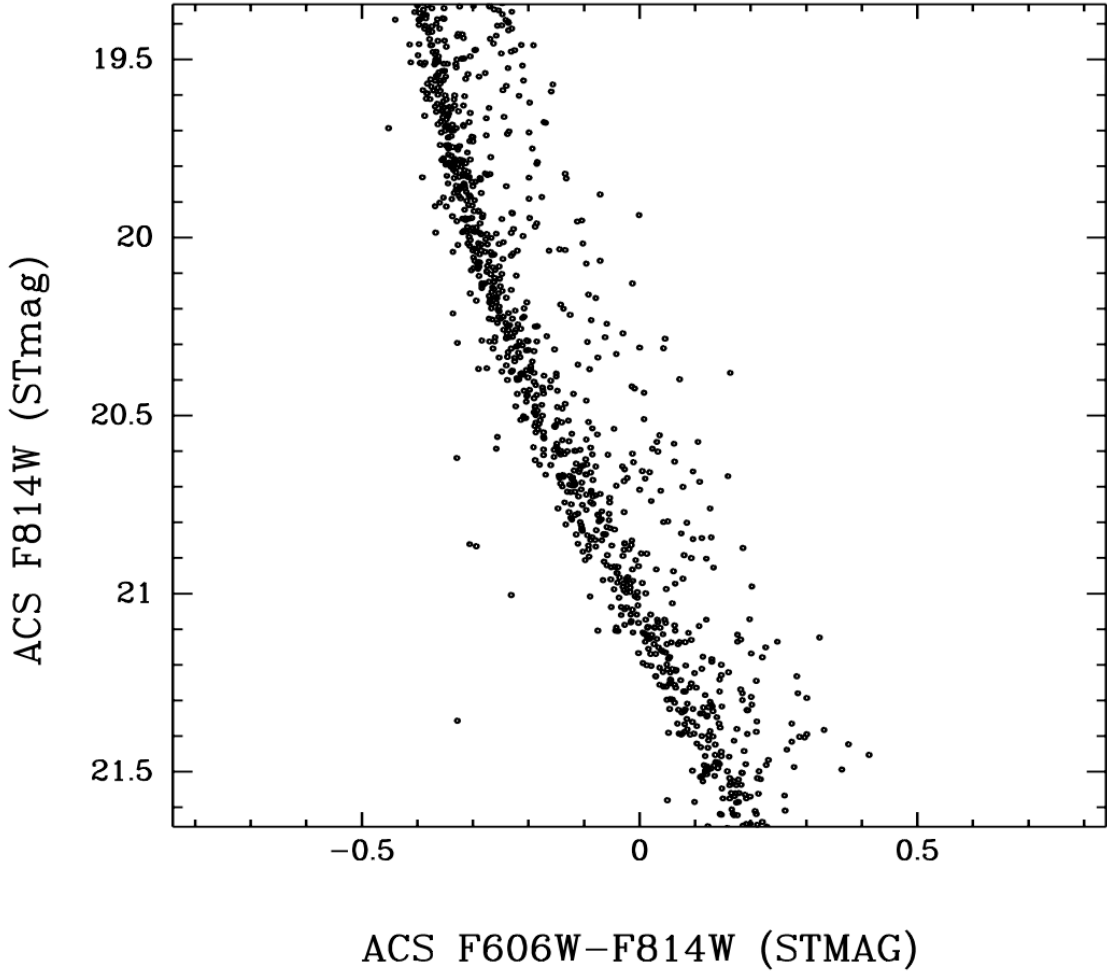


Figure 12 ACS color-magnitude diagram of 47 Tucanae derived from aperture photometry from calibration program 10737. The y-axis spans the same range of magnitudes shown in Figure 11 and corresponds to a total range in color (V-I) of approximately 0.6 magnitudes along the main sequence. The population of points to the right of the main sequence are most likely binary stars.

#### 4. Conclusions and Recommendations

1. This study shows that the ACS/WFC and WFC3/UVIS photometric calibration agree with the white dwarf models to within  $1.2 \pm 1.8 \%$  on average for the 8 bandpasses in this study.

The consistency of the photometric calibration of ACS/WFC and WFC3/UVIS is within  $\pm 0.5\%$  for F814W, F775W, F606W and F475W, and within  $\pm 1\%$  for F625W and F850LP. The apparent difference in the calibration is 2% for F555W and 6% for UVIS/F438W and ACS/F435W.

2. The instrument to instrument magnitude differences between similar passbands depend on the stellar spectral type and range from  $\Delta\text{mag} = -0.06$  to  $0.02$ , with the exception of F814W, where  $\Delta\text{mag} \sim -0.001\text{mag}$ .

Comparing the ACS/WFC to WFC3/UVIS mean flux for stars having a range of spectral types shows a color dependence. The WFC to UVIS F814W color dependence is of  $\pm 0.02$  mags for F814W, F775W, F475W and F606W. For the other filters the range is -0.06 to +0.02 mags.

3. Observations of the 47 Tucanae cluster with ACS/WFC and WFC3/UVIS1 and UVIS2 confirm the results using synthetic photometry of CALSPEC stars.

#### **Caveats:**

This analysis is based on the WFC3/UVIS 2017 chip-dependent calibration and related synthetic photometry tables which are derived by averaging together 6 years of standard star observations; and on the 2016 ACS/WFC calibration. It does not take into account either spatial or temporal variations. The rate of temporal change in CCD response is unique to each detector, and is wavelength dependent (cf. Shanahan et al. 2017). The decline in absolute sensitivity is as large as 1% since WFC3's installation in 2009. ACS/WFC decline in sensitivity since 2009 is  $\sim 0.1\%$ /year (Bohlin 2016) *Therefore, users who require accurate results are strongly recommended to use the calibrations appropriate for the epoch of observation.*

WFC3/UVIS time-dependent calibrations will be available soon, similar to those already available for the ACS channels.

#### **Acknowledgements.**

We thank R. Bohlin for his careful reading of the original typescript and whose comments greatly improved this report.

## **5. References**

The instrument science reports referred to in this study are either the most recent and/or relevant reports on the instruments' photometric calibration. Please check the ACS webpages at [www.stsci.edu/hst/acs](http://www.stsci.edu/hst/acs) and the WFC3 webpages at [www.stsci.edu/hst/wfc3](http://www.stsci.edu/hst/wfc3) for additional information.

Hayes D.S. and Latham, D.W., 1975, ApJ, 197, 53. A rediscussion of the atmospheric extinction and the absolute spectral-energy distribution of VEGA.

Price S.D., Paxson C., Engelke C., Murdock, T., 2004, AJ, 128, 889. Spectral Irradiance Calibration in the Infrared. XV. Absolute Calibration of Standard Stars by Experiments on the Midcourse Space Experiment.

Bohlin, Ralph C.; Gordon, Karl D.; Tremblay, P.-E., 2014, PASP, 126, 711. Techniques and Review of Absolute Flux Calibration from the Ultraviolet to the Mid-Infrared.

Deustua, S., Kent S., Smith, J.A., 2013, Absolute Calibration of Astronomical Flux Standards in Planets, Stars and Stellar Systems, by Oswalt, Terry D.; Bond, Howard E., ISBN 978-94-007-5617-5. Springer Science+Business Media Dordrecht, 2013, p. 375

*Some references for ACS photometric calibration:*

- R. Bohlin, 2016, ACS ISR 2016-03 Perfecting the Photometric Calibration of the ACS CCD Cameras and AJ
- R. Bohlin, 2012, ACS ISR 2012-01 Flux Calibration of the ACS CCD Cameras IV. Absolute Fluxes
- L. Ubeda and J. Anderson ISR 2013-01 Study of the evolution of the ACS/WFC sensitivity loss

*For information on the WFC3/UVIS photometric calibration:*

- S.E. Deustua, J. Mack, V. Bajaj, H. Khandrika WFC3 ISR 2017-14: WFC3/UVIS Updated 2017 Chip-Dependent Inverse Sensitivity Values
- C. E. Shanahan, C. M. Gosmeyer, S. Baggett WFC3 ISR 2017-15: 2017 Update on the WFC3/UVIS Stability and Contamination Monitor
- J. Mack, T. Dahlen, E. Sabbi, & A. S. Bowers WFC3 ISR 2016-04: UVIS 2.0: Chip-Dependent Flats
- S.E. Deustua, J. Mack, A.S. Bowers, S. Baggett, V. Bajaj, T. Dahlen, M. Durbin, C. Gosmeyer, H. Gunning, D. Hammer, G. Hartig, H. Khandrika J. MacKenty, R. Ryan, E. Sabbi, M. Sosey WFC3 ISR 2016-03: UVIS 2.0 Chip-dependent Inverse Sensitivity Values
- S.E. Deustua WFC3 ISR 2017-07: Updated WFC3/UVIS Chip Dependent SYNPHOT/PYSYNPHOT Files

*PySynphot:*

- Lim, P. L., Diaz, R. I., & Laidler, V. 2015, PySynphot User's Guide (Baltimore, MD: STScI), <https://pysynphot.readthedocs.io/en/latest/>.



## Appendix. Photometric Calibration Comparison between WFC3/UVIS1 and WFC3/UVIS2

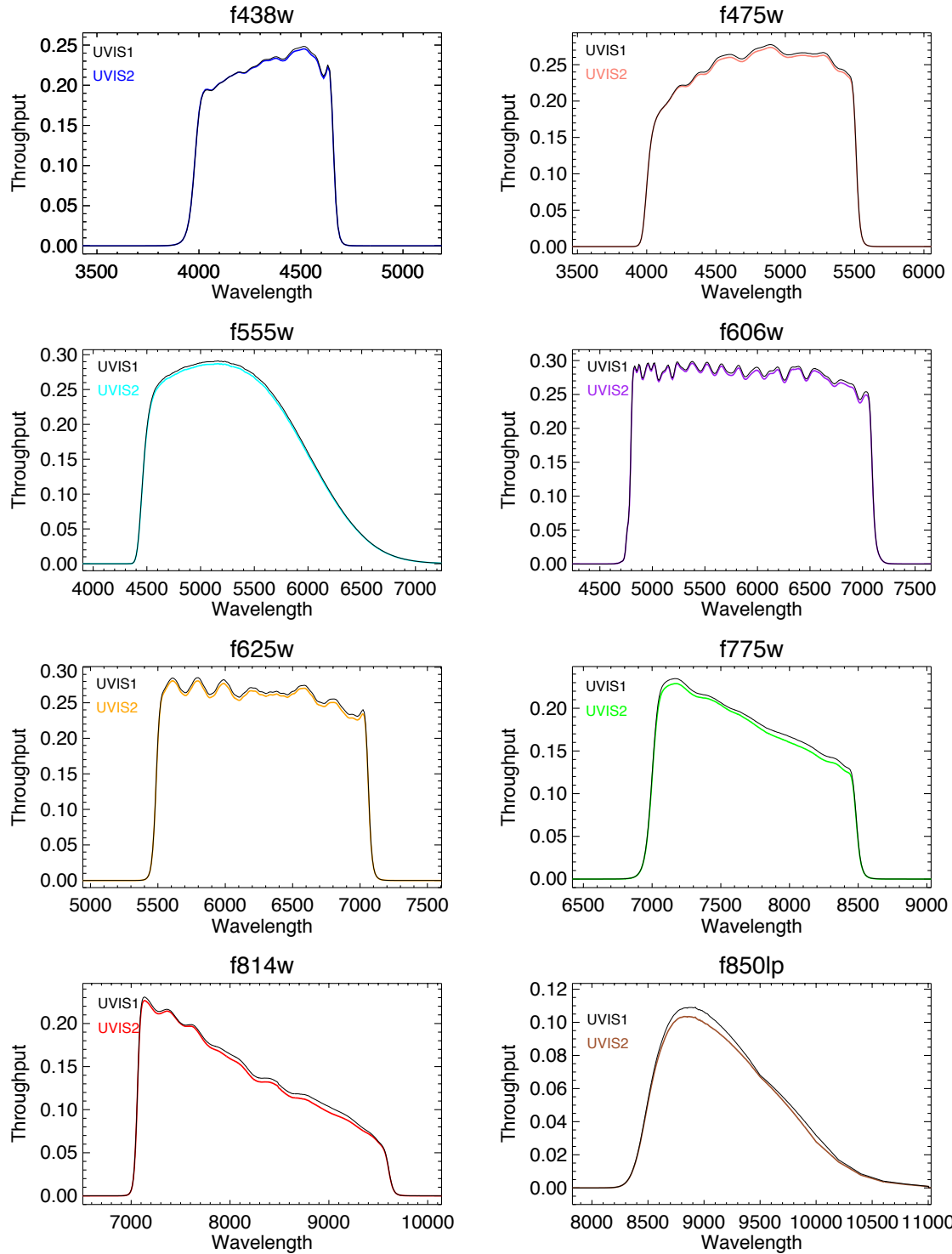


Figure 14. UVIS1 and UVIS2 bandpasses for the eight filters in the study are similar; UVIS1 has slightly higher throughput, most noticeable in F814W and F850LP. The photometric calibration accuracy is the same for both UVIS1 and UVIS2, but the effective wavelength and mean flux in the same filter will be slightly different in the two detectors (see Table 2).



*Appendix: Tables for the ACS/WFC to WFC3/UVIS1 color transformations*

| STAR        | WFC-UVIS1 |        |        |         |         |         |         |         |         |         |         |
|-------------|-----------|--------|--------|---------|---------|---------|---------|---------|---------|---------|---------|
|             | B-I       | B-V    | V-I    | F438W   | F475W   | F555W   | F606W   | F625W   | F775W   | F814W   | F850LP  |
|             | mag       | mag    | mag    | mag     | mag     | mag     | mag     | mag     | mag     | mag     | mag     |
| 10LAC       | -0.424    | -0.195 | -0.186 | -0.0480 | -0.0067 | 0.0065  | 0.0044  | 0.0061  | 0.0018  | -0.0017 | -0.0277 |
| 1732526     | 0.244     | 0.118  | 0.095  | 0.0010  | 0.0036  | -0.0088 | -0.0020 | -0.0040 | -0.0013 | -0.0004 | -0.0014 |
| 1740346     | 0.402     | 0.173  | 0.173  | -0.0037 | 0.0049  | -0.0153 | -0.0032 | -0.0078 | -0.0025 | -0.0007 | -0.0013 |
| 1743045     | 0.565     | 0.242  | 0.242  | -0.0093 | 0.0063  | -0.0215 | -0.0045 | -0.0111 | -0.0034 | -0.0010 | -0.0006 |
| 1757132     | 0.543     | 0.240  | 0.224  | -0.0076 | 0.0063  | -0.0188 | -0.0047 | -0.0112 | -0.0032 | -0.0008 | -0.0001 |
| 1802271     | 0.109     | 0.054  | 0.043  | 0.0009  | 0.0017  | -0.0044 | -0.0008 | -0.0018 | -0.0008 | -0.0002 | 0.0005  |
| 1805292     | 0.242     | 0.114  | 0.098  | -0.0002 | 0.0035  | -0.0092 | -0.0020 | -0.0040 | -0.0014 | -0.0004 | 0.0006  |
| 1808347     | 0.415     | 0.174  | 0.184  | -0.0034 | 0.0050  | -0.0147 | -0.0033 | -0.0083 | -0.0025 | -0.0008 | -0.0009 |
| 1812095     | 0.413     | 0.197  | 0.162  | 0.0035  | 0.0065  | -0.0158 | -0.0032 | -0.0076 | -0.0019 | -0.0005 | 0.0008  |
| AGK         | -0.703    | -0.314 | -0.314 | -0.0547 | -0.0095 | 0.0211  | 0.0060  | 0.0116  | 0.0035  | -0.0017 | -0.0366 |
| ALPHA Lyr   | 0.000     | 0.000  | 0.000  | 0.0000  | 0.0000  | 0.0000  | 0.0000  | 0.0000  | 0.0000  | 0.0000  | 0.0000  |
| BD02D3375   | 1.129     | 0.436  | 0.516  | -0.0333 | 0.0101  | -0.0400 | -0.0088 | -0.0247 | -0.0074 | -0.0014 | 0.0041  |
| BD21D0607   | 1.038     | 0.407  | 0.470  | -0.0308 | 0.0099  | -0.0377 | -0.0080 | -0.0225 | -0.0068 | -0.0015 | 0.0025  |
| BD26D2606   | 1.050     | 0.404  | 0.481  | -0.0325 | 0.0093  | -0.0382 | -0.0082 | -0.0230 | -0.0070 | -0.0014 | 0.0033  |
| BD29D2091   | 1.195     | 0.479  | 0.530  | -0.0358 | 0.0118  | -0.0419 | -0.0093 | -0.0256 | -0.0075 | -0.0015 | 0.0041  |
| BD54D1216   | 1.081     | 0.430  | 0.483  | -0.0316 | 0.0106  | -0.0388 | -0.0084 | -0.0234 | -0.0068 | -0.0015 | 0.0026  |
| BD60D1753   | 0.036     | 0.019  | 0.013  | -0.0007 | 0.0006  | -0.0015 | -0.0003 | -0.0005 | -0.0004 | 0.0000  | -0.0001 |
| BD17D4708   | 1.057     | 0.410  | 0.481  | -0.0292 | 0.0100  | -0.0371 | -0.0084 | -0.0231 | -0.0068 | -0.0014 | 0.0032  |
| FEIGE110    | -0.641    | -0.283 | -0.288 | -0.0499 | -0.0085 | 0.0174  | 0.0056  | 0.0106  | 0.0028  | -0.0016 | -0.0342 |
| G191B2B     | -0.677    | -0.302 | -0.302 | -0.0551 | -0.0091 | 0.0215  | 0.0054  | 0.0114  | 0.0033  | -0.0017 | -0.0360 |
| GD153       | -0.615    | -0.262 | -0.284 | -0.0511 | -0.0077 | 0.0198  | 0.0046  | 0.0113  | 0.0033  | -0.0017 | -0.0352 |
| GD71        | -0.571    | -0.235 | -0.270 | -0.0468 | -0.0066 | 0.0192  | 0.0040  | 0.0114  | 0.0032  | -0.0017 | -0.0348 |
| GRW_70D5824 | -0.323    | -0.090 | -0.184 | -0.0275 | -0.0014 | 0.0124  | 0.0018  | 0.0101  | 0.0023  | -0.0018 | -0.0310 |
| HD009051    | 1.791     | 0.778  | 0.741  | -0.0432 | 0.0201  | -0.0533 | -0.0142 | -0.0344 | -0.0103 | -0.0010 | 0.0153  |
| HD031128    | 1.125     | 0.453  | 0.499  | -0.0321 | 0.0114  | -0.0401 | -0.0087 | -0.0241 | -0.0070 | -0.0014 | 0.0032  |
| HD074000    | 1.000     | 0.386  | 0.458  | -0.0304 | 0.0090  | -0.0366 | -0.0076 | -0.0221 | -0.0067 | -0.0015 | 0.0016  |
| HD106252    | 1.284     | 0.579  | 0.512  | -0.0239 | 0.0159  | -0.0425 | -0.0099 | -0.0260 | -0.0068 | -0.0014 | 0.0037  |
| HD111980    | 1.204     | 0.496  | 0.523  | -0.0315 | 0.0131  | -0.0412 | -0.0094 | -0.0252 | -0.0073 | -0.0014 | 0.0051  |
| HD116405    | -0.125    | -0.057 | -0.054 | -0.0098 | -0.0019 | 0.0030  | 0.0013  | 0.0020  | 0.0003  | -0.0002 | -0.0035 |
| HD14943     | 0.389     | 0.181  | 0.155  | -0.0018 | 0.0058  | -0.0140 | -0.0033 | -0.0075 | -0.0020 | -0.0007 | -0.0008 |
| HD158485    | 0.286     | 0.128  | 0.121  | 0.0000  | 0.0039  | -0.0102 | -0.0024 | -0.0053 | -0.0018 | -0.0006 | 0.0001  |
| HD159222    | 1.323     | 0.609  | 0.516  | -0.0217 | 0.0166  | -0.0434 | -0.0102 | -0.0267 | -0.0068 | -0.0014 | 0.0047  |
| HD160617    | 1.094     | 0.429  | 0.494  | -0.0312 | 0.0103  | -0.0389 | -0.0085 | -0.0239 | -0.0070 | -0.0014 | 0.0030  |
| HD163466    | 0.402     | 0.175  | 0.171  | -0.0022 | 0.0053  | -0.0139 | -0.0034 | -0.0081 | -0.0024 | -0.0008 | 0.0001  |
| HD165459    | 0.244     | 0.120  | 0.093  | 0.0013  | 0.0040  | -0.0083 | -0.0023 | -0.0042 | -0.0014 | -0.0006 | -0.0019 |
| HD180609    | 0.250     | 0.109  | 0.109  | -0.0002 | 0.0032  | -0.0094 | -0.0019 | -0.0047 | -0.0017 | -0.0004 | 0.0013  |
| HD185975    | 1.419     | 0.653  | 0.554  | -0.0244 | 0.0177  | -0.0459 | -0.0109 | -0.0283 | -0.0073 | -0.0013 | 0.0060  |
| HD200654    | 1.459     | 0.575  | 0.654  | -0.0410 | 0.0136  | -0.0472 | -0.0116 | -0.0306 | -0.0094 | -0.0012 | 0.0108  |

|               |        |        |         |         |         |         |         |         |         |         |         |
|---------------|--------|--------|---------|---------|---------|---------|---------|---------|---------|---------|---------|
| HD205905      | 1.294  | 0.592  | 0.509   | -0.0222 | 0.0162  | -0.0427 | -0.0100 | -0.0263 | -0.0067 | -0.0014 | 0.0041  |
| HD37725       | 0.354  | 0.162  | 0.145   | -0.0010 | 0.0049  | -0.0130 | -0.0030 | -0.0065 | -0.0021 | -0.0008 | -0.0012 |
| HD37962       | 1.350  | 0.609  | 0.540   | -0.0270 | 0.0167  | -0.0437 | -0.0105 | -0.0268 | -0.0072 | -0.0013 | 0.0056  |
| HD38949       | 1.208  | 0.538  | 0.487   | -0.0248 | 0.0148  | -0.0412 | -0.0095 | -0.0246 | -0.0064 | -0.0014 | 0.0026  |
| KSI2CETI      | -0.103 | -0.049 | -0.042  | -0.0057 | -0.0015 | 0.0033  | 0.0009  | 0.0019  | 0.0002  | -0.0001 | -0.0019 |
| LAMLEP        | -0.530 | -0.234 | -0.239  | -0.0463 | -0.0076 | 0.0126  | 0.0050  | 0.0086  | 0.0023  | -0.0015 | -0.0283 |
| MUCOL         | -0.579 | -0.254 | -0.261  | -0.0490 | -0.0082 | 0.0134  | 0.0056  | 0.0093  | 0.0027  | -0.0017 | -0.0309 |
| P041C         | 1.294  | 0.587  | 0.513   | -0.0229 | 0.0161  | -0.0429 | -0.0101 | -0.0262 | -0.0067 | -0.0015 | 0.0034  |
| P177D         | 1.380  | 0.622  | 0.552   | -0.0239 | 0.0170  | -0.0442 | -0.0108 | -0.0274 | -0.0075 | -0.0015 | 0.0056  |
| P330E         | 1.362  | 0.607  | 0.550   | -0.0284 | 0.0166  | -0.0441 | -0.0106 | -0.0272 | -0.0073 | -0.0014 | 0.0054  |
| SIRIUS        | -0.047 | -0.014 | -0.027  | -0.0009 | -0.0003 | 0.0018  | 0.0002  | 0.0014  | 0.0000  | -0.0003 | -0.0043 |
| SNAP1         | -0.403 | -0.191 | -0.165  | -0.0343 | -0.0056 | 0.0116  | 0.0039  | 0.0075  | 0.0013  | -0.0014 | -0.0220 |
| SNAP2         | 1.407  | 0.631  | 0.564   | -0.0294 | 0.0176  | -0.0460 | -0.0112 | -0.0273 | -0.0075 | -0.0012 | 0.0062  |
| SUN_REFERENCE | 1.366  | 0.623  | 0.532   | -0.0232 | 0.0169  | -0.0434 | -0.0108 | -0.0280 | -0.0072 | -0.0017 | 0.0012  |
| WD1057 +719   | -0.541 | -0.256 | -0.2670 | -0.0521 | -0.0079 | 0.0247  | 0.0011  | -0.0021 | 0.0079  | 0.0003  | -0.0384 |
| WD1657 +343   | -0.627 | -0.278 | -0.2810 | -0.0531 | -0.0085 | 0.0188  | 0.0051  | 0.0110  | 0.0030  | -0.0019 | -0.0369 |

Table 4. The ACS/WFC color (F435W-F814W), (F435W-F606W) and (F606W-F814W) for each star is given in columns 2-4, and the magnitude difference between similar filters, ACS/WFC-WFC3/UVIS1, in the VegaMAG system is tabulated in columns 5-12.

| WFC – UVIS1 |             |         |             |         |             |         |
|-------------|-------------|---------|-------------|---------|-------------|---------|
| ACS Color   | F435W-F814W |         | F435W-F606W |         | F606W-F814W |         |
| Filter      | a           | b       | a           | b       | a           | b       |
| F475W       | -0.0004     | 0.0117  | -0.0003     | 0.0273  | 0.0000      | 0.0270  |
|             | ±0.0002     | ±0.0003 | ±0.0001     | ±0.0003 | ±0.0003     | ±0.0008 |
| F555W       | -0.0014     | -0.0323 | -0.0016     | -0.0742 | -0.0020     | -0.0756 |
|             | ±0.0004     | ±0.0004 | ±0.0006     | ±0.0015 | ±0.0003     | ±0.0009 |
| F606W       | 0.0000      | -0.0079 | -0.0001     | -0.0181 | -0.0002     | -0.0183 |
|             | ±0.0001     | ±0.0001 | ±0.0001     | ±0.0003 | ±0.0001     | ±0.0003 |
| F625W       | -0.0010     | -0.0194 | -0.0012     | -0.0445 | -0.0015     | -0.0453 |
|             | ±0.0003     | ±0.0004 | ±0.0005     | ±0.0012 | ±0.0004     | ±0.0009 |
| F775W       | -0.0001     | -0.0057 | -0.0002     | -0.0129 | -0.0002     | -0.0133 |
|             | ±0.0001     | ±0.0002 | ±0.0002     | ±0.0005 | ±0.0001     | ±0.0003 |
| F814W       | -0.0010     | -0.0001 | -0.0010     | -0.0003 | -0.0010     | -0.0003 |
|             | ±0.0001     | ±0.0001 | ±0.0001     | ±0.0002 | ±0.0001     | ±0.0002 |

Table 5. Coefficients for a linear fit,  $y=a(\pm \sigma_a)+b(\pm \sigma_b)x$ , where  $x$  is the stellar color and  $y$  is the difference in magnitude between instruments (ACS-UVIS1) and  $\sigma_a$  and  $\sigma_b$  are the uncertainties in the coefficients. The fits are to the points in Figure 8 that are based on the synthetic photometry for the CALSPEC stars in Table 2.

| WFC-UVIS1 |           |             |             |             |             |             |             |
|-----------|-----------|-------------|-------------|-------------|-------------|-------------|-------------|
| Filter    | ACS Color | F435w-F814W |             | F435W-F606W |             | F606W-F814W |             |
|           | segment   | a           | b           | a           | b           | a           | b           |
| F850LP    | blue      | -0.001      | 0.056       | -0.003      | 0.119       | 0.000       | 0.127       |
|           |           | $\pm 0.002$ | $\pm 0.005$ | $\pm 0.003$ | $\pm 0.014$ | $\pm 0.002$ | $\pm 0.008$ |
|           | mid       | -0.001      | 0.001       | 0.000       | 0.002       | 0.000       | -0.002      |
|           |           | $< 0.001$   | $\pm 0.001$ | $< 0.001$   | $\pm 0.003$ | 0.000       | $\pm 0.003$ |
|           | red       | -0.013      | 0.014       | -0.006      | 0.019       | -0.020      | 0.047       |
|           |           | $\pm 0.003$ | $\pm 0.002$ | $< 0.001$   | $\pm 0.003$ | $\pm 0.002$ | $\pm 0.003$ |

Table 6 Linear fit coefficients for the three segments in the instrument color in Figure 8 vs. stellar color diagrams for the F850LP bandpass. As in Table 5,  $y=a(\pm \sigma_a) + b(\pm \sigma_b)x$ , where  $x$  is the stellar color and  $y$  is the difference in magnitude between instruments (ACS-UVIS1) and  $\sigma_a$  and  $\sigma_b$  are the uncertainties in the coefficients. The fits are to the points in Figure 8 and are based on the synthetic photometry for the CALSPEC stars in Table 2.

*Appendix: Tables for the ACS/WFC to WFC3/UVIS2 color transformations*

| STAR        | WFC-UVIS2 |        |        |         |         |         |         |         |         |         |         |
|-------------|-----------|--------|--------|---------|---------|---------|---------|---------|---------|---------|---------|
|             | B-I       | B-V    | V-I    | F438W   | F475W   | F555W   | F606W   | F625W   | F775W   | F814W   | F850LP  |
|             | mag       | mag    | mag    | mag     | mag     | mag     | mag     | mag     | mag     | mag     | mag     |
| 10LAC       | -0.424    | -0.195 | -0.186 | -0.0476 | -0.0064 | 0.0066  | 0.0046  | 0.0061  | 0.0019  | -0.0009 | -0.0272 |
| 1732526     | 0.244     | 0.118  | 0.095  | 0.0007  | 0.0034  | -0.0089 | -0.0021 | -0.0040 | -0.0014 | -0.0006 | -0.0014 |
| 1740346     | 0.402     | 0.173  | 0.173  | -0.0039 | 0.0046  | -0.0154 | -0.0034 | -0.0079 | -0.0027 | -0.0011 | -0.0014 |
| 1743045     | 0.565     | 0.242  | 0.242  | -0.0097 | 0.0060  | -0.0216 | -0.0047 | -0.0112 | -0.0037 | -0.0014 | -0.0008 |
| 1757132     | 0.543     | 0.240  | 0.224  | -0.0081 | 0.0059  | -0.0190 | -0.0049 | -0.0113 | -0.0034 | -0.0013 | -0.0002 |
| 1802271     | 0.109     | 0.054  | 0.043  | 0.0008  | 0.0016  | -0.0045 | -0.0008 | -0.0019 | -0.0009 | -0.0003 | 0.0004  |
| 1805292     | 0.242     | 0.114  | 0.098  | -0.0004 | 0.0033  | -0.0092 | -0.0021 | -0.0041 | -0.0015 | -0.0006 | 0.0005  |
| 1808347     | 0.415     | 0.174  | 0.184  | -0.0037 | 0.0047  | -0.0149 | -0.0035 | -0.0084 | -0.0027 | -0.0011 | -0.0009 |
| 1812095     | 0.413     | 0.197  | 0.162  | 0.0031  | 0.0062  | -0.0159 | -0.0034 | -0.0077 | -0.0021 | -0.0008 | 0.0007  |
| AGK         | -0.703    | -0.314 | -0.314 | -0.0541 | -0.0090 | 0.0212  | 0.0063  | 0.0117  | 0.0038  | -0.0005 | -0.0359 |
| ALPHA Lyr   | 0.000     | 0.000  | 0.000  | 0.0000  | 0.0000  | 0.0000  | 0.0000  | 0.0000  | 0.0000  | 0.0000  | 0.0000  |
| BD02D3375   | 1.129     | 0.436  | 0.516  | -0.0338 | 0.0095  | -0.0403 | -0.0094 | -0.0249 | -0.0079 | -0.0026 | 0.0037  |
| BD21D0607   | 1.038     | 0.407  | 0.470  | -0.0313 | 0.0094  | -0.0379 | -0.0086 | -0.0227 | -0.0072 | -0.0025 | 0.0023  |
| BD26D2606   | 1.050     | 0.404  | 0.481  | -0.0330 | 0.0087  | -0.0385 | -0.0087 | -0.0232 | -0.0075 | -0.0025 | 0.0030  |
| BD29D2091   | 1.195     | 0.479  | 0.530  | -0.0364 | 0.0112  | -0.0422 | -0.0100 | -0.0258 | -0.0080 | -0.0027 | 0.0037  |
| BD54D1216   | 1.081     | 0.430  | 0.483  | -0.0321 | 0.0101  | -0.0391 | -0.0089 | -0.0236 | -0.0073 | -0.0025 | 0.0023  |
| BD60D1753   | 0.036     | 0.019  | 0.013  | -0.0008 | 0.0006  | -0.0015 | -0.0003 | -0.0005 | -0.0004 | -0.0001 | -0.0001 |
| BD17D4708   | 1.057     | 0.410  | 0.481  | -0.0297 | 0.0094  | -0.0374 | -0.0090 | -0.0233 | -0.0073 | -0.0025 | 0.0028  |
| FEIGE110    | -0.641    | -0.283 | -0.288 | -0.0494 | -0.0081 | 0.0176  | 0.0059  | 0.0107  | 0.0031  | -0.0005 | -0.0335 |
| G191B2B     | -0.677    | -0.302 | -0.302 | -0.0546 | -0.0087 | 0.0217  | 0.0057  | 0.0115  | 0.0036  | -0.0006 | -0.0353 |
| GD153       | -0.615    | -0.262 | -0.284 | -0.0507 | -0.0073 | 0.0199  | 0.0049  | 0.0115  | 0.0035  | -0.0006 | -0.0345 |
| GD71        | -0.571    | -0.235 | -0.270 | -0.0465 | -0.0063 | 0.0194  | 0.0043  | 0.0115  | 0.0034  | -0.0006 | -0.0342 |
| GRW_70D5824 | -0.323    | -0.090 | -0.184 | -0.0276 | -0.0014 | 0.0125  | 0.0019  | 0.0101  | 0.0024  | -0.0009 | -0.0305 |
| HD009051    | 1.791     | 0.778  | 0.741  | -0.0443 | 0.0191  | -0.0538 | -0.0151 | -0.0347 | -0.0111 | -0.0029 | 0.0147  |
| HD031128    | 1.125     | 0.453  | 0.499  | -0.0326 | 0.0108  | -0.0404 | -0.0093 | -0.0243 | -0.0075 | -0.0026 | 0.0028  |
| HD074000    | 1.000     | 0.386  | 0.458  | -0.0309 | 0.0085  | -0.0368 | -0.0082 | -0.0223 | -0.0072 | -0.0025 | 0.0013  |
| HD106252    | 1.284     | 0.579  | 0.512  | -0.0249 | 0.0151  | -0.0429 | -0.0106 | -0.0262 | -0.0073 | -0.0025 | 0.0033  |
| HD111980    | 1.204     | 0.496  | 0.523  | -0.0322 | 0.0124  | -0.0416 | -0.0100 | -0.0254 | -0.0078 | -0.0025 | 0.0047  |
| HD116405    | -0.125    | -0.057 | -0.054 | -0.0096 | -0.0019 | 0.0030  | 0.0013  | 0.0020  | 0.0004  | -0.0001 | -0.0034 |
| HD14943     | 0.389     | 0.181  | 0.155  | -0.0022 | 0.0055  | -0.0141 | -0.0035 | -0.0076 | -0.0022 | -0.0010 | -0.0009 |
| HD158485    | 0.286     | 0.128  | 0.121  | -0.0003 | 0.0037  | -0.0102 | -0.0025 | -0.0054 | -0.0020 | -0.0008 | 0.0000  |
| HD159222    | 1.323     | 0.609  | 0.516  | -0.0227 | 0.0158  | -0.0438 | -0.0109 | -0.0269 | -0.0073 | -0.0025 | 0.0042  |
| HD160617    | 1.094     | 0.429  | 0.494  | -0.0317 | 0.0097  | -0.0392 | -0.0091 | -0.0241 | -0.0075 | -0.0025 | 0.0027  |
| HD163466    | 0.402     | 0.175  | 0.171  | -0.0026 | 0.0051  | -0.0140 | -0.0036 | -0.0082 | -0.0026 | -0.0011 | 0.0000  |
| HD165459    | 0.244     | 0.120  | 0.093  | 0.0010  | 0.0038  | -0.0084 | -0.0024 | -0.0042 | -0.0014 | -0.0007 | -0.0019 |
| HD180609    | 0.250     | 0.109  | 0.109  | -0.0004 | 0.0030  | -0.0095 | -0.0020 | -0.0048 | -0.0018 | -0.0006 | 0.0012  |
| HD185975    | 1.419     | 0.653  | 0.554  | -0.0255 | 0.0168  | -0.0463 | -0.0117 | -0.0285 | -0.0078 | -0.0026 | 0.0056  |
| HD200654    | 1.459     | 0.575  | 0.654  | -0.0417 | 0.0128  | -0.0476 | -0.0124 | -0.0308 | -0.0101 | -0.0028 | 0.0103  |

|               |        |        |         |         |         |         |         |         |         |         |         |
|---------------|--------|--------|---------|---------|---------|---------|---------|---------|---------|---------|---------|
| HD205905      | 1.294  | 0.592  | 0.509   | -0.0232 | 0.0153  | -0.0430 | -0.0107 | -0.0265 | -0.0072 | -0.0025 | 0.0037  |
| HD37725       | 0.354  | 0.162  | 0.145   | -0.0013 | 0.0047  | -0.0131 | -0.0032 | -0.0065 | -0.0023 | -0.0010 | -0.0013 |
| HD37962       | 1.350  | 0.609  | 0.540   | -0.0280 | 0.0159  | -0.0441 | -0.0112 | -0.0270 | -0.0078 | -0.0025 | 0.0052  |
| HD38949       | 1.208  | 0.538  | 0.487   | -0.0257 | 0.0141  | -0.0415 | -0.0101 | -0.0248 | -0.0069 | -0.0024 | 0.0022  |
| KSI2CETI      | -0.103 | -0.049 | -0.042  | -0.0056 | -0.0014 | 0.0033  | 0.0010  | 0.0019  | 0.0002  | 0.0000  | -0.0018 |
| LAMLEP        | -0.530 | -0.234 | -0.239  | -0.0458 | -0.0072 | 0.0127  | 0.0053  | 0.0087  | 0.0025  | -0.0006 | -0.0277 |
| MUCOL         | -0.579 | -0.254 | -0.261  | -0.0485 | -0.0079 | 0.0136  | 0.0058  | 0.0094  | 0.0029  | -0.0007 | -0.0303 |
| P041C         | 1.294  | 0.587  | 0.513   | -0.0239 | 0.0153  | -0.0433 | -0.0107 | -0.0264 | -0.0073 | -0.0026 | 0.0030  |
| P177D         | 1.380  | 0.622  | 0.552   | -0.0249 | 0.0162  | -0.0446 | -0.0115 | -0.0276 | -0.0080 | -0.0027 | 0.0052  |
| P330E         | 1.362  | 0.607  | 0.550   | -0.0294 | 0.0158  | -0.0445 | -0.0113 | -0.0275 | -0.0078 | -0.0026 | 0.0050  |
| SIRIUS        | -0.047 | -0.014 | -0.027  | -0.0009 | -0.0003 | 0.0018  | 0.0002  | 0.0014  | 0.0000  | -0.0001 | -0.0041 |
| SNAP1         | -0.403 | -0.191 | -0.165  | -0.0339 | -0.0054 | 0.0117  | 0.0041  | 0.0076  | 0.0014  | -0.0007 | -0.0217 |
| SNAP2         | 1.407  | 0.631  | 0.564   | -0.0304 | 0.0167  | -0.0464 | -0.0119 | -0.0275 | -0.0081 | -0.0024 | 0.0058  |
| SUN_REFERENCE | 1.366  | 0.623  | 0.532   | -0.0242 | 0.0161  | -0.0438 | -0.0115 | -0.0282 | -0.0078 | -0.0028 | 0.0008  |
| WD1057 +719   | -0.541 | -0.256 | -0.2670 | -0.0517 | -0.0075 | 0.0248  | 0.0013  | -0.0020 | 0.0086  | 0.0023  | -0.0377 |
| WD1657 +343   | -0.627 | -0.278 | -0.2810 | -0.0527 | -0.0081 | 0.0189  | 0.0054  | 0.0111  | 0.0032  | -0.0007 | -0.0362 |

Table 7. The ACS/WFC color (B-I=F435W-F814W), (B-V=F435W-F606W) and (V-I=F606W-F814W) for each star is given in columns 2-4, and the magnitude difference between similar filters, ACS/WFC-WFC3/UVIS2, in the VegaMAG system is tabulated in columns 5-12

| WFC-UVIS2 |             |         |             |         |            |         |
|-----------|-------------|---------|-------------|---------|------------|---------|
| ACS Color | F435W-F814W |         | F435W-F606W |         | F606-F814W |         |
| Filter    | a           | b       | a           | b       | a          | b       |
| f475w     | -0.0004     | 0.0111  | -0.0004     | 0.0259  | -0.0001    | 0.0257  |
|           | ±0.0002     | ±0.0003 | ±0.0001     | ±0.0003 | ±0.0003    | ±0.0008 |
| f555w     | -0.0014     | -0.0326 | -0.0016     | -0.0748 | -0.0021    | -0.0762 |
|           | ±0.0004     | ±0.0004 | ±0.0006     | ±0.0015 | ±0.0003    | ±0.0009 |
| f606w     | 0.0000      | -0.0084 | -0.0001     | -0.0192 | -0.0002    | -0.0194 |
|           | ±0.0001     | ±0.0001 | ±0.0001     | ±0.0003 | ±0.0001    | ±0.0003 |
| f625w     | -0.0010     | -0.0196 | -0.0012     | -0.0449 | -0.0015    | -0.0457 |
|           | ±0.0003     | ±0.0004 | ±0.0005     | ±0.0012 | ±0.0004    | ±0.0009 |
| f775w     | -0.0001     | -0.0061 | -0.0002     | -0.0139 | -0.0002    | -0.0143 |
| f         | ±0.0002     | ±0.0002 | ±0.0002     | ±0.0005 | ±0.0001    | ±0.0003 |
| f814w     | -0.0008     | -0.0013 | -0.0008     | -0.0030 | -0.0008    | -0.0031 |
|           | ±0.0001     | ±0.0001 | ±0.0001     | ±0.0002 | ±0.0001    | ±0.0002 |

Table 8. Coefficients for a linear fit,  $y=a(\pm \sigma_a)+b(\pm \sigma_b)x$ , where  $x$  is the stellar color and  $y$  is the difference in magnitude between instruments (ACS/WFC and WFC3/UVIS2) and  $\sigma_a$  and  $\sigma_b$  are the uncertainties in the coefficients. The fits are to the points in Figure 8 and are based on synthetic photometry for the CALSPEC stars in Table 2.

|           |         | WFC-UVIS2   |             |             |             |             |             |
|-----------|---------|-------------|-------------|-------------|-------------|-------------|-------------|
| ACS Color |         | F435-F814   |             | f435-F606   |             | F606-F814   |             |
| Filter    | segment | a           | b           | a           | b           | a           | b           |
| F850LP    | blue    | -0.001      | 0.055       | -0.003      | 0.117       | 0.000       | 0.125       |
|           |         | $\pm 0.002$ | $\pm 0.005$ | $\pm 0.003$ | $\pm 0.014$ | $\pm 0.002$ | $\pm 0.008$ |
|           | mid     | -0.001      | 0.001       | 0.000       | 0.001       | 0.000       | -0.003      |
|           |         | $< 0.001$   | $\pm 0.001$ | $< 0.001$   | $\pm 0.003$ | $< 0.001$   | $< 0.001$   |
|           | red     | -0.013      | 0.014       | -0.006      | 0.018       | -0.020      | 0.046       |
|           |         | $\pm 0.003$ | $\pm 0.002$ | $\pm 0.003$ | $\pm 0.005$ | $\pm 0.002$ | $\pm 0.003$ |

Table 9. Linear fit coefficients for the three segments in the instrument color vs. stellar color diagrams for the F850LP bandpass in Figure 8. As in Table 8,  $y=a(\pm \sigma_a) + b(\pm \sigma_b)x$ , where  $x$  is the stellar color and  $y$  is the difference in magnitude between instruments (ACS/WFC and WFC3/UVIS2) and  $\sigma_a$  and  $\sigma_b$  are the uncertainties in the coefficients. The fits are to the points in Figure 8 and are based synthetic photometry for the CALSPEC stars in Table 2.

## Appendix: Color Transformation Figures for ACS/WFC to WFC3/UVIS2

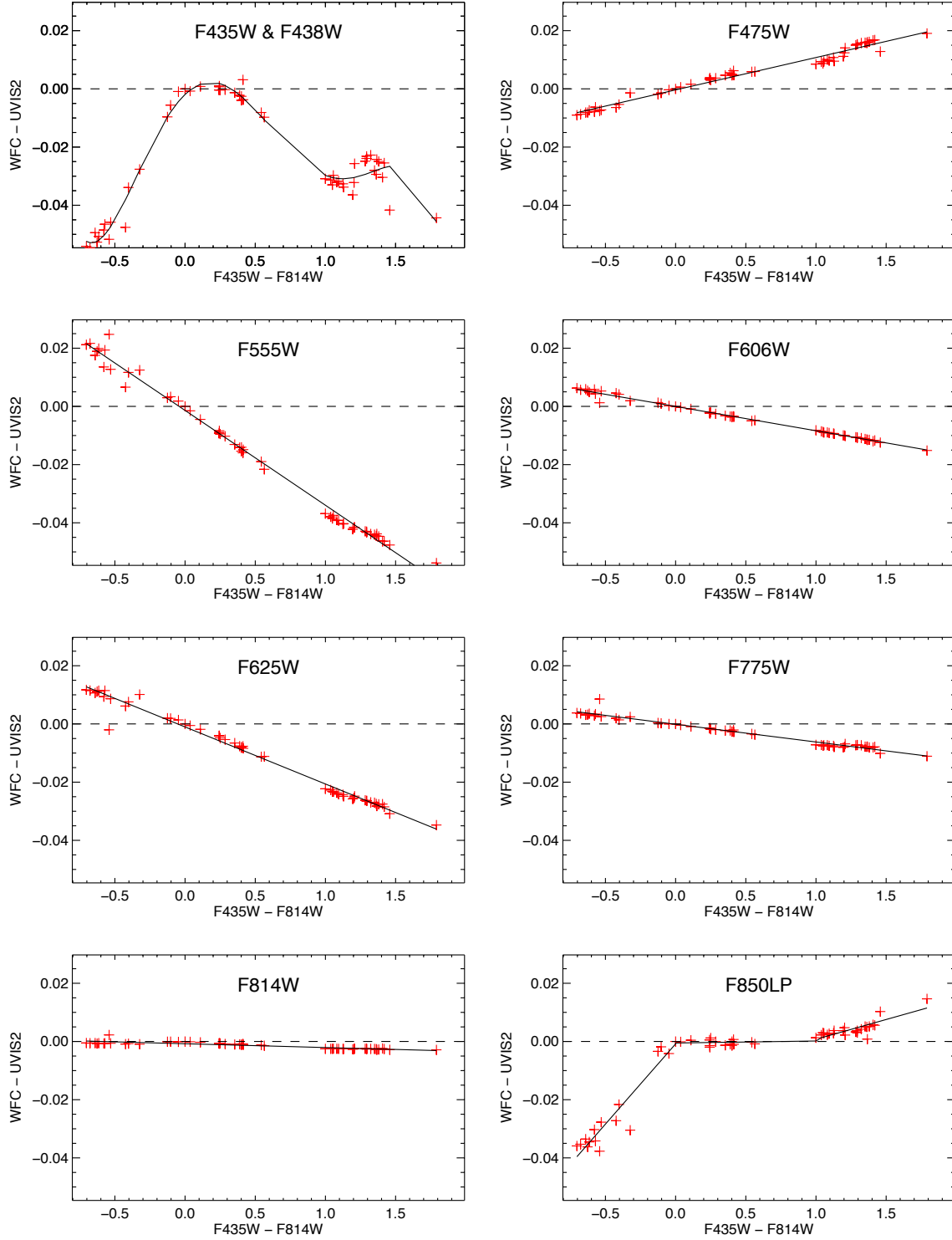


Figure 13a. Plots of stellar color (ACS F435W-F814W) versus the difference between the ACS/WFC and WFC3/UVIS2 magnitudes for each of the similar bandpasses. The relationship is linear except for F435W-F438W where a 5<sup>th</sup> order polynomial was used, and, F850LP where a 3-line fit seemed appropriate

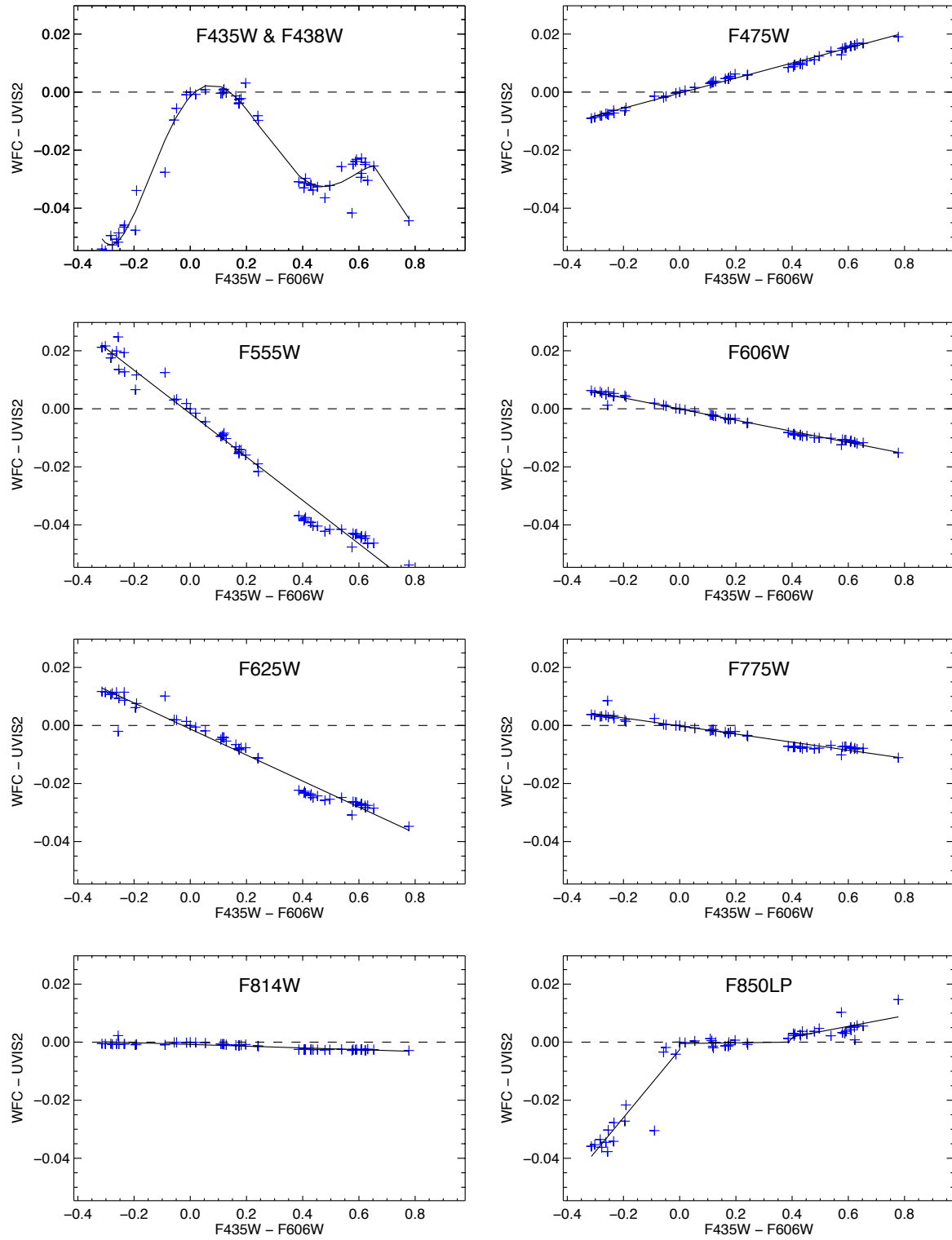


Figure 13b. As in Figure 13a but plotted against ACS/WFC F435W - F606W, roughly comparable to B-V



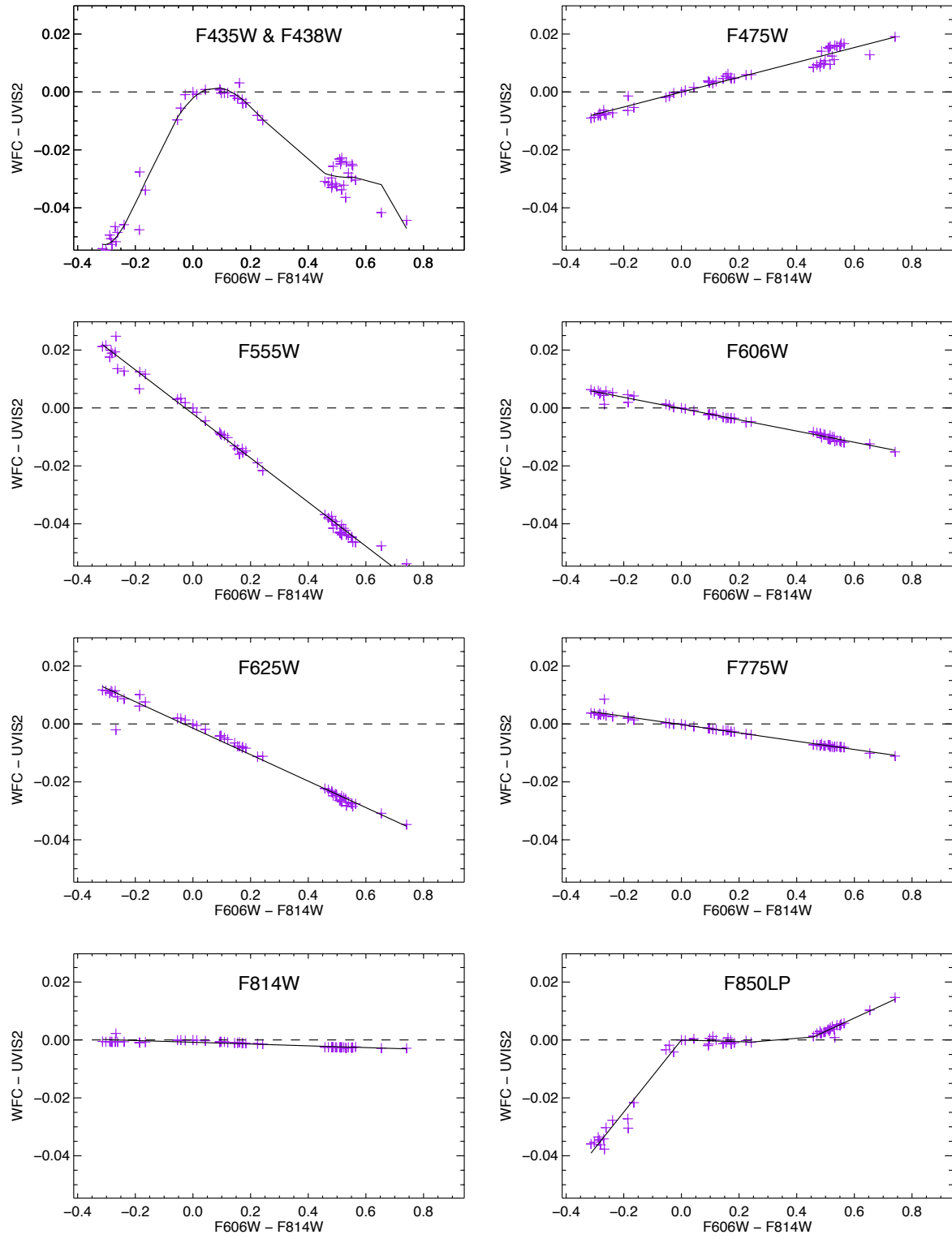


Figure 13c. As in Figure 13a but plotted against ACS/WFC  $F606W - F814W$ , roughly comparable to V-I